

Inaugural-Dissertation zur Erlangung der Doktorwürde der Tierärztlichen
Fakultät der Ludwig-Maximilians-Universität München

**Antisense oligonucleotide- and CRISPR-Cas9-mediated
rescue of mRNA splicing for a deep intronic *CLRN1*
mutation**

Von Anna-Lena Panagiotopoulos
aus Recklinghausen in Nordrhein-Westfalen

München 2021

Aus dem Veterinärwissenschaftlichen Department der Tierärztlichen
Fakultät der Ludwig-Maximilians-Universität München

Lehrstuhl für Pharmakologie, Toxikologie und Pharmazie

Arbeit angefertigt unter der Leitung von Univ.-Prof. Dr. Hermann Ammer

Angefertigt am Zentrum für Pharmaforschung
der Fakultät für Chemie und Pharmazie der Ludwig-Maximilians-
Universität München

Mentor: PD Dr. Elvir Becirovic

Gedruckt mit Genehmigung der Tierärztlichen Fakultät der
Ludwig-Maximilians-Universität München

Dekan: Univ.-Prof. Dr. Reinhard K. Straubinger, Ph.D.

Berichterstatter: Univ.-Prof. Dr. Hermann Ammer

Koreferent: Univ.-Prof. Dr. Laurent Frantz

Tag der Promotion: 06. Februar 2021

Widmung

Meinen Eltern, Geschwistern, Patentante und Loui

Die vorliegende Arbeit wurde gemäß § 6 Abs. 2 der Promotionsordnung für die Tierärztliche Fakultät der Ludwig-Maximilians-Universität München in kumulativer Form verfasst.

Folgende wissenschaftliche Arbeiten sind in dieser Dissertationsschrift enthalten:

Anna-Lena Panagiotopoulos, Nina Karguth, Marina Pavlou, Sybille Böhm, Gilles Gasparoni, Jörn Walter, Alexander Graf, Helmut Blum, Martin Biel, Lisa Maria Riedmayr, and Elvir Becirovic. **Antisense oligonucleotide- and CRISPR-Cas9-mediated rescue of mRNA splicing for a deep intronic *CLRN1* mutation (2020) Molecular Therapy - Nucleic Acids.**

Table of contents

1	Introduction	1
1.1	Retinal Anatomy	1
1.2	Retinitis pigmentosa	2
1.3	Degenerative retinal disorders in mammals	4
1.4	Usher syndrome	6
1.5	Pre-mRNA splicing	7
1.6	Splice mutations	8
1.7	<i>CLRN1</i>	9
1.8	Therapy of USH3	11
1.9	CRISPR-Cas9	12
1.10	Antisense-Oligonucleotides	13
2	Publication: Antisense oligonucleotide- and CRISPR-Cas9-mediated rescue of mRNA splicing for a deep intronic <i>CLRN1</i> mutation	15
3	Discussion	59
4	References	62

1 Introduction

1.1 Retinal Anatomy

A typical feature of the vertebral eye is its invert structure. Light has to pass different layers until it reaches the light sensitive layer of the eye, called retina. The retina is a 0.5 mm thin layer, which represents a part of the central nervous system. It consists of three distinct layers, which house six major cell types including photoreceptors, bipolar cells, horizontal cells, amacrine cells and ganglion cells. Müller glia, are the only non-neural retinal cell type which provide metabolic and homeostatic support [1], [2]. There are two types of photoreceptors, rods and cones. Their cell bodies form the outer nuclear layer (ONL) and are embedded in the retinal pigment epithelium (RPE). Retinal pigment epithelium cells are involved in the regeneration of the visual pigment and they are responsible for digestion of light-detecting compartments of photoreceptors, called outer segments (Figure 1) [2]. The inner nuclear layer houses the cell bodies of bipolar, horizontal and amacrine cells. The latter two form synapses with the neighboured cells [3]. Rods and cones are able to convert light energy to membrane potential change, a process called phototransduction which results in neurotransmitter release at the synapse [1]. Rods account for 95% of the photoreceptors in the human retina. They enable dim light vision, whereas cones mediate colour and daylight vision. Rods and cones are composed of an inner and outer segment (Figure 2). Outer segments contain different proteins and pigments essential for phototransduction [4]. By contrast, inner segments contain many mitochondria to meet the high energy requirements of photoreceptors.

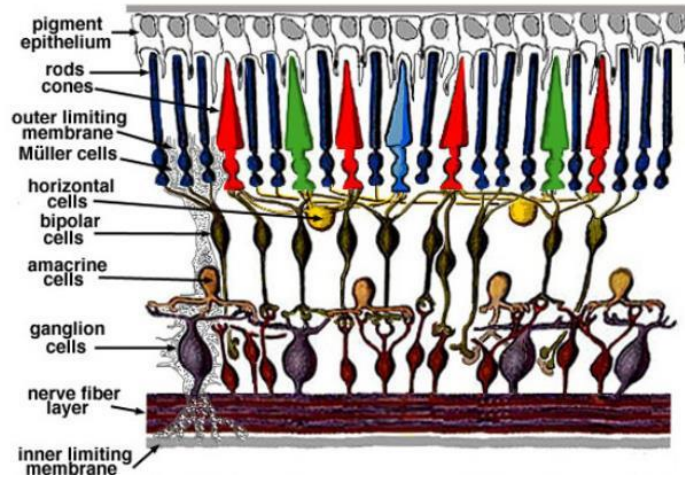


Figure 1: Anatomy of the retina. For further explanation, see text. Figure taken from Kolb 2005.

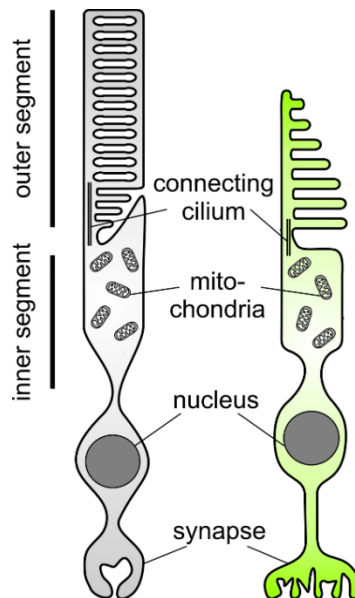


Figure 2: Rod (l.) and cone (r.) photoreceptor structure. Both cell types can be divided into an outer and inner segment and the synaptic ending. Inner and outer segment are coupled by the connecting cilium.

1.2 Retinitis pigmentosa

Retinitis pigmentosa (RP) is the most common genetic cause for blindness worldwide and affects one in 3.000 - 8.000 people [5]. The disease can be syndromic or non-syndromic with X-chromosomal, autosomal dominant or autosomal recessive inheritance [6]. In the case of syndromic RP, in addition to blindness the patients present with additional symptoms in other tissues or organs [6]. One prominent example for syndromic RP is the Usher syndrome, as

described in detail in the section below. So far, mutations in over 60 different genes have been associated with RP [7]. Most of them affect genes expressed in photoreceptors and retinal pigment epithelium, making it very challenging to establish common treatment strategies [6]. The phenotypic variability of RP depends on many factors including the type of inheritance, genetic background of the patient, or mutation type [8], [9]. The degeneration of photoreceptor cells starts in the mid-fringe of the retina and expands towards the macula lutea and fovea, leading to progressive visual loss [5]. As a consequence, the outer nuclear layer gets thinner and eventually gets almost entirely depleted [6], [10]. Patients become aware of the pathology when they notice symptoms like night blindness, progressive constriction of visual fields and peripheral vision loss. Symptoms get worse over time and end in tunnel vision or complete blindness [7]. This is primarily caused by the degeneration of rods followed by the secondary loss of cones [2], [11]. In later stages, when cones become affected, patients will also suffer from bad colour and daylight vision, as well as from photophobia, which is an intolerance to light exposure [6], [9]. Finally, loss of central vision will manifest [2]. In patient's fundus, bone-spicule shaped pigments in the mid-periphery and shrinking of retinal vessels can be observed. In the end stage of RP, no or very weak signal is present in patients' electroretinograms (Figure 3) [6]. RP equivalents also exist in other mammals, such as dogs where the clinical picture is led progressive retinal atrophy (PRA) [9]

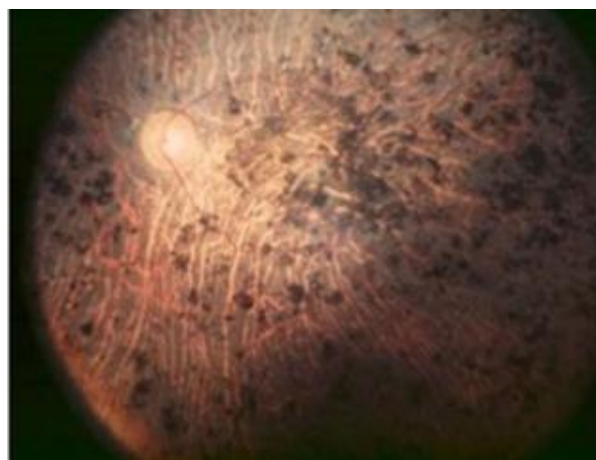


Figure 3: End stage fundus of patients carrying Retinitis pigmentosa. Black dots represent retinal pigmentation. Figure taken from Ali et al. 2017.

1.3 Degenerative retinal disorders in mammals

During the last decades a variety of naturally occurring gene mutations causing retinal disorders with a stationary or progressive clinical picture could be identified in mammals [12], [13]. Around 29 different mutations are described in literature to cause degenerative or developmental retinal disorders in dogs (Figure 4) [13]. The Briard carries a naturally occurring mutation located in the *RPE65* gene, which belongs to the group of stationary retinal disorders. This mutation leads to severe visual impairment similar to what can be observed in humans suffering from Leber congenital amaurosis (LCA) [14]. RPE65 is known to be involved in retinoid metabolism. Mutations in *RPE65* lead to an accumulation of all-*trans*-retinyl esters, very low levels of the visual pigment rhodopsin, a dysfunction of rod photoreceptors as well as inclusions in the RPE in mice [15]–[18]. Acland et al. could restore vision in *RPE65*^{-/-} deficient dogs by a subretinal injection of adeno-associated virus serotype 2 (AAV2/2) expressing a correct copy of the disease gene. On the basis of their findings it became possible to develop the first gene therapy drug, called Luxturna™, for patients suffering from biallelic mutations in *RPE65* [19]. Based on the clinical phenotype observed in affected dogs, progressive retinal atrophies (PRAs) can be denoted as the canine equivalent of retinitis pigmentosa (RP) where mutations in the related genes lead to photoreceptor decay over time [9]. PRAs are characterized by initial loss of rod function followed by the degeneration of cones. Typically, the first clinical signs are night blindness, followed by vision impairment under daylight conditions. PRAs can be subdivided into early- and late-onset forms. The Papillon suffers from PRA caused by a naturally occurring *CNGB1* mutation. The clinical phenotype in these dogs is similar to that in humans suffering from RP. Consequently, this dog is an appropriate large animal model for autosomal recessive retinitis pigmentosa [9], [13]. Another breed also became important in science, namely the Miniature longhaired dachshund, which hosts a *RPGRIP1* gene mutation. Due to his small size and the clinical observations found in affected individuals, this dog model helped to develop treatment strategies for human retinal disorders like LCA, RP and cone-rod degeneration (CRD) [20]–[22]. Because of the similarities between dog and man, with regard to the clinical features of RP, the size of the eye as well as the

photoreceptor density, dogs are very attractive animal models for RP and other retinal disorders [9], [23]. Inherited retinal dystrophies have also been described in other animals and often resemble the human clinical phenotypes. One example is the homozygous Appaloosa horse which carries a naturally occurring mutation in *TRIPM1* gene (also known as melastatin). The TRIPM-1 protein is expressed in ON bipolar cells of the retina and in the skin and plays an essential role for bipolar cell signalling and melanocyte function. Mutations in this gene lead to a downregulation or rather absence of a functional protein, a phenotype which is called complete congenital stationary night blindness (cCSNB) [24], [25]. Affected horses typically show impaired night vision from birth [26]. Inherited retinal dystrophies have also been found in other small animals, such as cats [27]. Cases of progressive retinal atrophy as well as rod-cone dysplasia are described in breeds like the Abyssinian, Somali, Persian, or Bengal cat [27]–[30]. The breed of the Abyssinian cat harbors a naturally occurring single-base deletion in the *CRX* gene, which results in a premature stop codon and early onset rod cone dysplasia (rdy) [31], [32]. First clinical signs like nystagmus or mydriasis occur early in life and dysplasia affects rods and cones equally. Retinal dysplasia is caused by improper development of photoreceptor cells [27], [28], [33]. Another example of inherited retinal diseases in Abyssinian cats is the progressive rod-cone degeneration (*rdAc*) attributable to mutations in the *CEP290* gene, a gene causing RP or LCA in humans [27], [28]. In these animals starting from an age of 1.5 to 2 years, rods start to degenerate followed by a loss of cones [34], [35]. The tapetal layer starts to change its colour and reflectivity accompanied by vascular sustenance in more peripheral areas of the fundus. In later stages retinal thinning and hypereflectivity can be observed, finally ending in complete loss of visual function at the age of 3 to 4 years [28]. In addition to the rdAc, other cat models for inherited retinal dystrophies also exist, such as the Bengal cat showing an early-onset autosomal recessive blindness (Figure 5 and 6), or the Persian cat model for autosomal recessive rod-cone dysplasia [27], [29], [36].

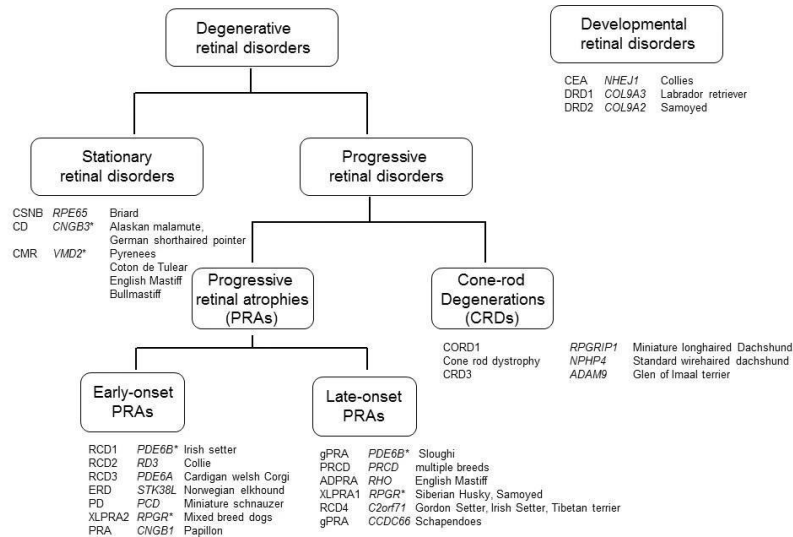


Figure 4: Categorization of canine retinal disorders. Figure taken from Mellersh CS. 2014.

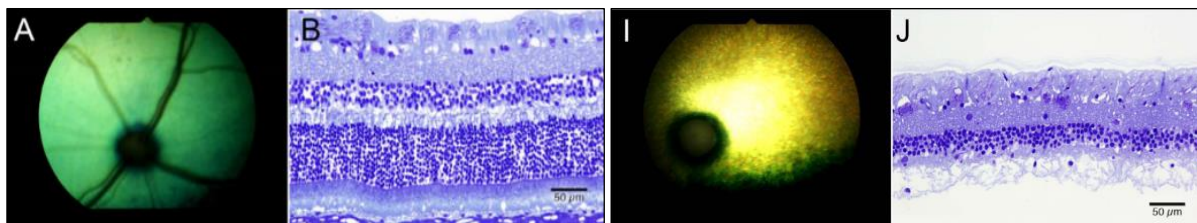


Figure 5 (l.) and 6 (r.): Color fundus photographs and photomicrographs of Bengal cats suffering from PRA. Area centralis from an obligate carrier Bengal kitten at 8 weeks of age (l.). Funduscopic signs usually become evident between 8 to 20 weeks of age and comprise a generalized increase in granularity and subsequent reflectivity of the tapetum lucidum, among mild retinal vascular attenuation (A,B) and I, J Bengal kitten fundus at 62 weeks of age (r.). Complete retinal degeneration, apparent as tapetal hyperreflectivity and absence of retinal arterioles or venules can be seen. Figure taken from Ofri et al. 2015.

1.4 Usher syndrome

The Usher syndrome (USH) is an autosomal recessive disease characterized by deafness, vision loss due to RP, and occasional vestibular dysfunction [37]. With a prevalence in the range of approximately 1: 6.000, USH is the most common cause for hereditary deaf-blindness worldwide [38], [39]. Depending on the onset and severeness of the disease, there are three different types of the Usher syndrome. Type 1 (USH1) is the most severe form and characterized by congenital deafness, vestibular dysfunction and early-onset RP [2]. Mutations in six different genes were found in USH1 patients. *Myosin VIIA* (USH1B), *Harmonin* (USH1C), *Cadherin-23* (USH1D), *Protocadherin-15* (USH1F), *Sans* (USH1G) and *Cib2* [40]–[45].

Patients with USH2 suffer from moderate to severe hearing loss, normal vestibular function and RP starting in the second decade of life. USH2 is caused by mutations in the genes *Usherin*, *NBC-3*, *VLGR1b* or *Whirlin* [2], [46]–[48]. Usher syndrome type 3 (USH3) is primarily caused by mutations in *USH3A* (also known as *CLRN1*), a gene encoding for the protein CLRN-1. Patients suffering from USH3 present with the most variable clinical phenotype which includes progressive RP, hearing loss and vestibular dysfunction [2]. Another gene associated with USH3 is *HARS* (histidyl-tRNA synthetase) [49]–[51].

USH3 accounts for 1-6% of all USH cases worldwide. However, its prevalence is highly enriched in some populations, such as the Ashkenazi Jews and the Finnish population (up to 40% of USH3 cases) [52], [53]. Most of the USH genes encode for large scaffold proteins responsible for the maintenance of the complex architecture of photoreceptor and hair cells, where they form multiprotein complexes [2]. Furthermore, these proteins are involved in cell adhesion, intracellular trafficking and G-protein- or Ca^{2+} -mediated signalling [2]. Hearing impairment can be efficiently treated by the help of cochlear implants, however, there is no curative therapy for the vision loss in USH patients [54]. One important factor hampering the development of treatment strategies for this disease is the lack of appropriate animal models (e.g. rodents) mimicking the visual phenotype of human patients. One explanation could be the missing photoreceptor calyceal process in rodents and/or other unknown mechanisms compensating the lack of functional USH proteins in these animals [55], [56]. As there is no therapy available for patients suffering from any of the USH subtypes there is an unmet need for development of new translational approaches.

1.5 Pre-mRNA splicing

In eukaryotic cells the transcription of DNA into pre-mRNA (messenger RNA) is followed by three important steps of RNA processing: pre-mRNA splicing, 5'-end capping and 3'-processing. These parts are required before mature mRNA can be exported to the cytoplasm as functional mRNA. Splicing of mRNA requires several critical elements, like the 5' (donor) and 3' (acceptor) splice sites, the consensus sequences, a branch site, a polypyrimidine

sequence and splicing enhancers. These elements are recognized by small nuclear ribonucleoproteins (snRNPs) (U1, U2, U4, U5 and U6) and other protein splicing factors, which are part of the so called spliceosome [57], [58]. In eukaryotic cells the pre-mRNA contains protein-coding regions (exons) and non-coding regions referred to as introns. During the splicing process the spliceosome reassembles on every intron and thereby catalyses a *trans*-esterification reaction, which leads to the removal of the intron and ligation of exons. This results in a mature mRNA which can be translated into functional proteins. To be identified by the splice machinery, the exon-intron boundaries contain specific recognition sequences called splice sites. These include a donor site (5' end of the intron), a branch site (near the 3' end of the intron) and an acceptor site (3' end of the intron).

1.6 Splice mutations

Approximately 15% of all disease-causing mutations are predicted to affect mRNA splicing [59]–[61]. As described in the previous section, an accurate splicing process requires the spliceosome and numerous of other splicing factors. Regularly, pre-mRNA splicing occurs with high fidelity, nevertheless pre-mRNA mis-splicing can happen in presence of disease-causing mutations [62]. Typically, splicing mutations are localized at the canonical donor and acceptor splice sites, which define the boundaries between exons and introns. However, aberrant splicing can also occur due to mutations in deep intronic parts of a pre-mRNA. This altered splicing process can happen via diverse mechanisms [63].

One of the most common mechanisms is the generation of novel exons in intronic regions. Due to diverse screening methods, e.g. Next generation sequencing (NGS), it became possible to identify deep intronic mutations in genes involved in the development of retinal dystrophies [63]–[68]. Because of the large number of deep intronic mutations identified within the last years, there is an unmet need for development of treatment strategies for this type of mutation.

1.7 CLRN1

CLRN1 is located on chromosome 3 and spans about 46 kb. It encodes a four-transmembrane protein (CLRIN-1) that belongs to the large family of tetraspanins and claudin (Figure 7) [50], [65], [69]. These tetraspanins form large interaction complexes with other neighbouring membrane proteins and serve various functions such as cell to cell adhesion, transmission of signals and scaffolding function [69], [70]. The exact molecular function of CLRIN-1 is largely unknown. However, the protein is expressed in the inner segments and ribbon synapses of photoreceptor cells, as well as in hair cells of the inner ear [53], [69].

CLRN1 gene can be expressed as different splice variants. The major splice variant contains exon 1 to 4 [51]. Nevertheless, the function of these splice variants is unclear, as some may underlie nonsense-mediated mRNA decay (NMD), because of premature stop codons, whereas others may be translated into functional proteins [39]. The mutation this work is dealing with, is a deep-intronic c.254-649T>G *CLRN1* mutation found in the Saudi Arabian population and is located between exon 0b and exon 1. The point mutation causes a new aberrant exon in intron 0b (230bp), which generates a novel donor splice site leading to a frame-shift and a premature stop codon (Figure 8). This results in either a shortened protein or an unstable transcript due to NMD. This finally is expected to result in severe changes or complete loss of *CLRN1* function [65]. This mutation is not the only mutation identified in *CLRN1* gene during the last decades as shown in the table below.

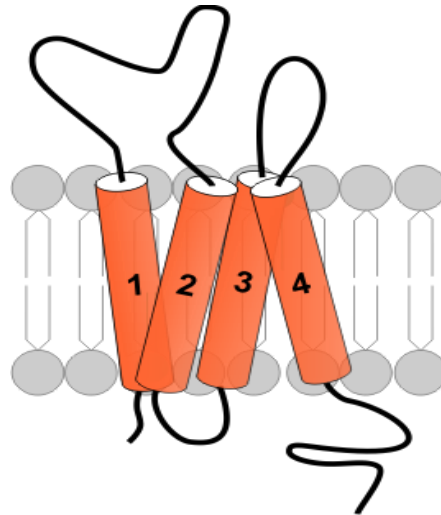


Figure 7: CLRN-1 protein structure. A four transmembrane protein located in the inner segments and synapses of photoreceptor cells. CLRN-1 belongs to the large family of tetraspanins and claudin.

Table 1: Mutations identified in *USH3A*.

Type of mutation	Nucleotide	Protein	Reference
Nonsense	c.300T → G	Y100X	[51]
Missense	c.131T → A	M44K	
Nonsense	c.528T → G	Y176X	[71]
Missense	c.165delC	N48I	
Missense	c.144T → G	N48K	
Missense	c. 359T → A	M120K	
Missense	c. 449T → C	L150P	
Missense	c.143T → G	N48K	[50]
Nonsense	c.189C → A	Y63X	
Missense	c.118T → G	C40G	[72]

Missense	c.359T → A	M120K	
Missense	c.368C → A	A123D	[73]
Missense	c.449T → C	L150P	
Substitution	c.254-1G → A	Unclear	[74]

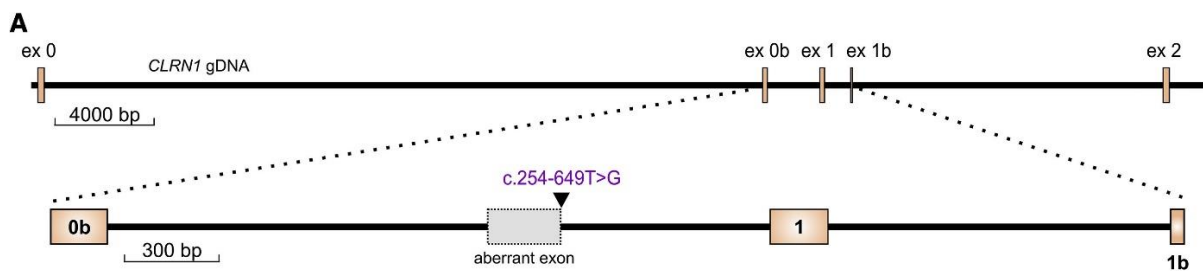


Figure 8: Scheme of the *CLRN1* gene encompassing exons 0 – 2. Lower panel, enlarged version of the gene region with deep intronic c.254-649T>G mutation, which generates an aberrant exon in intron 0b. Figure taken from Panagiotopoulos et al. 2020.

1.8 Therapy of USH3

Effective therapy of USH3 is rather challenging for several reasons. One of them is the incomplete or missing knowledge of the expression and function of this gene. In addition, for unknown reasons *CLRN1* KO mice do not develop a retinal phenotype [56]. The absence of faithful disease models hinders the development of novel gene therapies [75]. Moreover, *CLRN1* gene encodes a high number of different splice isoforms and thus encodes several transcripts, whose function is poorly understood [2], [39]. Gene delivery via recombinant adeno-associated viruses (rAAV) is the gold standard in gene therapy. Unfortunately, rAAVs have a limited packaging capacity of around 4.7kb or less. As a consequence only a single splice isoform can be delivered at once. Considering all these obstacles, there is an unmet need for developing strategies for the treatment of USH3 patients. The advantages of AONs and CRISPR-Cas9 gene editing are that both approaches do not depend on gene size or the presence of a single splice isoform.

1.9 CRISPR-Cas9

The CRISPR-Cas9 (clustered regularly interspaced short palindromic repeats) technology is an important technique to target, edit, modify and regulate any DNA sequence [76], [77]. CRISPR-Cas9 technology is based on a naturally occurring form of adaptive immune system which is found in many archaea and bacterial genomes [76], [78]. CRISPR-Cas9 was first described in *Streptococcus*, where numerous short direct repeats interspaced with short sequences were found in the genome. These antisense-RNAs derived from plasmids and viruses of past cell invasions [79]–[81]. This led to the assumption that these sequences could have a role in DNA repair or in gene regulation [82], [83]. Three different Cas-systems have been described so far, which differ in their molecular mechanisms to recognize and cleave nucleic acids [84], [85]. For CRISPR to be used in biotechnological applications, two components are required: a guide RNA (gRNA) and the CRISPR-associated endonuclease (Cas-endonuclease). The Cas9-endonuclease can e.g. be used to precisely cut out an intronic region containing the disease-causing mutation by introducing a double-strand break in this region [76], [86]. The other component, called gRNA recruits the Cas9-endonuclease to its target locus on DNA. The gRNA spans approximately 20 nucleotides and contains two important components: the trans-activating RNA (tracrRNA) at the 5' prime end that binds the Cas9-endonuclease and the CRISPR-RNA (crRNA) at the 3' prime end called protospacer that binds at the DNA target site. Both components are joined by a linker sequence [76]. Three nucleotides 3' to the protospacer the protospacer adjacent motif (PAM) is located, consisting of a NGG sequence that is crucial to initiate the hybridization between crRNA and the DNA target. As bacterial genomes do not contain such a PAM sequence, the endogenous bacterial DNA cannot be targeted by the CRISPR-Cas9 system [87]–[90]. After cleavage of the double strand the latter can be reassembled by non-homologous-end-joining (NHEJ) or by homology-directed-repair (HDR). Cas9-endonuclease, derived from *Streptococcus pyogenes* bacteria, consists of two nuclease domains, the HNH domain to cleave DNA strand complementary to the crRNA and the RuvC-like domain, which cleaves the complementary strand [91], [92].

This CRISPR-Cas9 gene editing technology, was already approved for first clinical trials designed to treat a deep intronic *CEP290* gene mutation, causing Leber congenital amaurosis in humans [93].

1.10 Antisense-Oligonucleotides

Antisense Oligonucleotides (AONs) are RNA-derived molecules consisting of 18 to 30 nucleotides [94], [95]. Commonly, they are used for the treatment of splice mutations or downregulation of gene expression. To become active, AONs have to pass molecular barriers like the cytoplasm or nucleoplasm [95]. After internalization they bind on pre-mRNA level through Watson-Crick base pairing. The alteration of splicing events via AONs can happen by several mechanisms, e.g. by inhibition of mRNA maturation, blocking of translation, RNase-H-mediated degradation or masking the splice factor recognition site [94], [96]–[98]. The stability and binding efficiency of AONs to the target mRNA, strongly depends on their chemistry as unmodified nucleic acids are prone to nuclease degradation. Moreover, the plasma protein binding capacity of unmodified AONs is very low, accelerating the elimination by the kidney [95], [97]. To improve the binding efficacy, tissue uptake, target affinity, nuclease avoidance, toxicity and half-life of AONs, some chemical modifications can be done. In the last few years, different generations of AONs were developed. For the studies presented in this work, AONs with a phosphothioate backbone were used, which are called phosphorothioate oligonucleotides (PTOs). They belong to first generation AONs, which contain a sulfur atom in the phosphodiester bond [99]. This modification should preserve the AONs against nuclease degradation, increase their solubility and improve the ability to bind the pre-mRNA [100]. Two other groups are the so-called phosphorodiamidate morpholino oligonucleotides (PMOs), which contain a ribose sugar or 2'-O-(2-Methoxyethyl)-oligoribonucleotides (2'-MOEs) [94]. Due to their small size, the easy way of design and the potential to apply them as naked molecules in cell culture as well as *in vivo*, AONs represent an attractive strategy for treatment of genetic disorders [101]. Furthermore, they are low in production costs and are expected to be uniformly distributed within the different cell types of the retina upon delivery [101].

Nevertheless, this approach has some important drawbacks, such as the requirement of constant supplementation throughout a patient's lifetime, as well as the dose-dependent toxicity [97]. Additionally, they can induce some adverse effects, such as coagulation or complement activation [102].

2 Publication

Antisense oligonucleotide- and CRISPR-Cas9-mediated rescue of mRNA splicing for a deep intronic *CLRN1* mutation

Antisense oligonucleotide- and CRISPR-Cas9-mediated rescue of mRNA splicing for a deep intronic *CLRN1* mutation

Anna-Lena Panagiotopoulos², Nina Karguth^{1,2}, Marina Pavlou^{2,3}, Sybille Böhm^{1,2}, Gilles Gasparoni⁴, Jörn Walter⁴, Alexander Graf⁵, Helmut Blum⁵, Martin Biel^{1,2}, Lisa Maria Riedmayr^{1,2*}, and Elvir Becirovic^{1,2*}

¹Center for Integrated Protein Science Munich CIPSM, Germany

²Department of Pharmacy - Center for Drug Research, Ludwig-Maximilians-Universität München, Germany

³Department of Ophthalmology - Munich Eye Hospital, Germany
Ludwig-Maximilians-Universität München, Germany

⁴Department of Genetics, Saarland University, Germany

⁵Gene Center Munich, Ludwig-Maximilians-Universität München, Germany

*Correspondence should be addressed to Elvir Becirovic, Department Pharmazie – Pharmakologie für Naturwissenschaften, Ludwig-Maximilians-Universität München, Butenandtstr. 5-13, D-81377 München, Germany, Phone: +49-89-2180-77905, FAX: +49-89-2180-77326, Email: elvir.becirovic@cup.lmu.de or

Lisa Maria Riedmayr, Department Pharmazie – Pharmakologie für Naturwissenschaften, Ludwig-Maximilians-Universität München, Butenandtstr. 5-13, D-81377 München, Germany, Phone: +49-89-2180-77316, FAX: +49-89-2180-77326, Email: lisa.riedmayr@cup.lmu.de

Short title

Splicing rescue of *CLRN1* mutation via AONs and CRISPR-Cas9

Keywords

CLRN1, mRNA splicing, antisense oligonucleotide, AON, CRISPR-Cas9, Usher syndrome, USH, USH3, splicing mutation, gene editing

Abstract

Mutations in *CLRN1* cause Usher syndrome type III (USH3A), a disease characterized by progressive hearing impairment, retinitis pigmentosa and vestibular dysfunction. Due to the lack of appropriate disease models, no efficient therapy for retinitis pigmentosa in USH patients exists so far. In addition, given the yet undefined functional role and expression of the different *CLRN1* splice isoforms in the retina, non-causative therapies like gene supplementation are unsuitable at this stage. Here, we focused on the recently identified deep intronic c.254-649T>G *CLRN1* splicing mutation and aimed to establish two causative treatment approaches: CRISPR-Cas9-mediated excision of the mutated intronic region and antisense oligonucleotide (AON)-mediated correction of mRNA splicing. The therapeutic potential of these approaches was validated in different cell types transiently or stably expressing *CLRN1* minigenes. Both approaches led to substantial correction of the splice defect. Surprisingly, however, no synergistic effect was detected when combining both methods. Finally, the injection of naked AONs into mice expressing the mutant *CLRN1* minigene in the retina also led to a significant splice rescue. We propose that both, AONs and CRISPR-Cas9, are suitable strategies to initiate advanced preclinical studies for treatment of USH3A patients.

Introduction

Usher syndrome is an autosomal recessive genetic disease characterized by deafness, vision loss due to retinitis pigmentosa (RP), and occasional vestibular dysfunction. In Usher syndrome type 3 (USH3A), these symptoms occur in a progressive and variable manner (1). USH3A is commonly associated with mutations in *CLRN1*, a gene encoding the four transmembrane domain protein Clarin-1 of largely unknown function. In the retina, the protein is suggested to be localized in the inner segments and ribbon synapses of photoreceptors, however, recent data also suggest expression in Müller glia cells (2, 3). This gene encodes many different splice isoforms, whose function is also poorly understood (4). *CLRN1* mutations have an estimated prevalence of 1:100,000 individuals worldwide, however, USH3 is the major USH subtype in the Ashkenazi Jewish and the Finnish population (5, 6). We have recently identified a novel deep intronic *CLRN1* founder mutation (c.254-649T>G) in the Saudi Arabian population (7). This splicing mutation generates an aberrant exon, which leads to a frameshift and a premature stop codon.

A substantial portion of all disease-causing mutations (>15 %) are predicted to affect mRNA splicing (8-10). Classical splicing mutations are localized at the canonical splice donor and acceptor sites defining the exon-intron boundaries. However, splicing mutations can also occur in deep intronic regions causing aberrant splicing via diverse mechanisms (11). Next generation sequencing (NGS) has made it possible to identify disease-causing deep intronic mutations in different genes associated with retinal dystrophies (7, 12-16). As the number of studies identifying deep intronic mutations in known or unknown genes increases, there is an unmet need for developing appropriate treatment strategies for this type of mutations.

Effective therapy of RP in USH patients is rather challenging for several reasons. First, many USH genes have a large (>4 kb) coding sequence or have a high number of splice isoforms encoding several protein-coding transcripts, whose function is hitherto poorly characterized (1). Currently, the recombinant adeno-associated virus (rAAV)-mediated gene delivery is the gold standard in gene therapy. However, due to the limited packaging capacity of rAAVs (≤ 4.7 kb), usually only a single splice isoform may be delivered at a time. Second, the commonly

used USH mouse models only reflect the hearing loss phenotype of human patients but not the neurodegenerative symptoms of retinitis pigmentosa. This lack of a faithful disease model hinders the development and testing of novel gene therapies aimed at the restoration of retinal structure and function (17). Given these obstacles, the development of alternative approaches for retinal gene therapy in USH patients is indispensable. For the treatment of intronic splicing mutations, causative approaches such as CRISPR-Cas9 or antisense oligonucleotides (AONs) appear very attractive as they do not depend on gene size or the presence of a single (major) splice isoform.

Herein, we set out to establish CRISPR-Cas9- and AON-based approaches to correct the splicing defect of the *CLRN1* c.254-649T>G mutation. We show that both approaches can substantially rescue the aberrant splicing in transfected or transduced cell lines. Finally, using AONs we obtained a significant rescue of mRNA splicing in the mouse retina expressing the mutant *CLRN1* minigene. These results offer a promising basis for advanced preclinical studies using CRISPR-Cas9 or AONs which could be advanced into the first clinical trials for USH3A.

Results

Editing of the CLRN1 locus using CRISPR-Cas9

The c.254-649T>G *CLRN1* mutation is located in intron 0b and generates a novel splice donor site (SDS), which results in the inclusion of an aberrant exon in the mature mRNA (Fig. 1A). To test the CRISPR-Cas9 efficiency for editing the *CLRN1* locus, we designed four single guide RNAs (sgRNAs, g1-g4) targeting regions flanking the mutation (Fig. 1B). To assess the efficiency for the two combinations, we transfected HEK293 cells with the plasmid expressing the *Streptococcus pyogenes* Cas9 and one of the two sgRNA pairs (g1 + g3 or g2 + g4, Fig. 1C). Both sgRNA combinations result in the excision of the DNA fragment in the native locus where the mutation is located. Compared to the g2 + g4 combination, which yielded rather low gene editing efficiency (4.36 % \pm 0.2 %), the g1 + g3 combination led to reasonably higher values under these conditions (21.22 % \pm 0.62 %) (Fig. 1D). Sanger sequencing of the PCR band amplified from the modified *CLRN1* locus revealed no substantial background in the electropherogram, as it would be expected in case of frequent insertions or deletions in the target region (Suppl. Fig. 1A, B).

Upon transfection, the transgene DNA is typically not taken up by all cells in the culture. To be able to calculate the actual editing efficiency of the native *CLRN1* locus in HEK293 cells more accurately, we transfected HEK293 cells with a *SpCas9*-T2A-EGFP cassette containing the g1 + g3 combination (Fig. 1E) and sorted the GFP positive (GFP+) cells using fluorescence-activated cell sorting (FACS) (Suppl. Fig. 1C). Indeed, gene editing efficiency in GFP+ cells was somewhat higher (25.9 % \pm 0.41 %, Fig 1F) compared to their unsorted counterparts.

Taken together, this CRISPR-Cas9 approach showed reasonable gene editing efficiency for the excision of the c.254-649T>G mutation from the native *CLRN1* locus in HEK293 cells.

Correction of CLRN1 mRNA splicing using AONs

To test the potential of the AONs for correction of aberrant splicing caused by the c.254-649T>G mutation, we designed five AONs (A1-A5) binding to different regions of the *CLRN1* transcript (Fig. 2A). The AONs were designed to either cover multiple exonic or intronic

splicing enhancer motifs or the created donor splice site (Suppl. Table 1). As we could not get access to patients' cells natively expressing the *CLRN1* mutation, we co-transfected HEK293 cells with AONs (250 nM each) and the wild type or mutant *CLRN1* minigenes encompassing exons 0b to 1b (Fig. 2B) (7). The RT-PCR from these cells revealed that only A2 could lead to a substantial splicing rescue resulting in $62.61\% \pm 2.05\%$ of correctly spliced transcript (Fig. 2C) as measured by densitometric analysis of PCR band intensities. We did not investigate the protein expression from these minigenes as they do not encode for any native protein product. Due to the large size of the introns in the *CLRN1* gene, any annotated transcript of this gene encoding a native protein would exceed the capacity of standard expression vectors.

In an attempt to further optimize the efficiency of A2, we tested three additional AONs by slightly changing their length or binding position (A2-A2.3, Suppl. Table 1). Among the modified versions tested, only A2.2 showed a trending but non-significant improvement in splicing rescue efficiency ($64.92\% \pm 1.36\%$) compared to A2 (Fig. 2D). We also detected two additional bands migrating between the bands which represent the correctly or aberrantly spliced *CLRN1* (Suppl. Fig.1D). These bands were also occasionally observed in cells expressing wild type or mutant *CLRN1* minigenes in the absence of AONs. Sequencing revealed that the lower one of the two bands results from the usage of an alternative splice donor site present in the native *CLRN1* transcript. The upper band represents a hybrid composed of the regularly spliced and the aberrantly spliced transcript. (Suppl. Fig.1E, F). These hybrids can occur during the PCR cycling conditions due to the fact that their single stranded components are largely built of complementary sequences (18).

To confirm the effects of the AON treatment on *CLRN1* mRNA splicing via another method, we carried out qRT-PCR using a primer combination that can specifically amplify the aberrantly spliced *CLRN1* transcripts and compared it to a primer combination capable of detecting both, the correctly and the aberrantly spliced variant. Quantification of the results revealed that the expression profile and the ratio of these two qRT-PCR products is very similar between cells expressing wild type and AON-treated c.254-649T>G *CLRN1* minigenes, but clearly differs

from the cells expressing the mutant *CLRN1* minigene alone ($0.023\% \pm 0.006\%$ for wt, $0.071\% \pm 0.015\%$ for mutant treated with A2.2 and $0.634\% \pm 0.036\%$ for mutant expressed alone, Suppl. Fig. 2A). Furthermore, we assessed a potential dose-dependence of AONs for *CLRN1* splicing correction. Using AON concentrations ranging between 50 - 250 nM, no apparent differences in splicing correction could be detected suggesting that A2.2 can act with high efficiency even at lower concentrations (Suppl. Fig 2B).

To test whether AON-based splicing correction might be cell type dependent, we performed similar experiments in two additional cell lines i.e. in mouse embryonic fibroblasts (MEFs) and in 661W cells, which are immortalized derivatives of murine cone photoreceptors (19). In both cell types, AON treatment led to a robust splicing correction although at lower efficiency than in HEK293 cells ($27.30\% \pm 4.03\%$ in MEF vs. $39.65\% \pm 0.43\%$ in 661W cells, respectively) (Suppl. Fig. 2C-D). Of note, AON treatment also led to an increase in the expression of additional bands, which are only weakly present in cells expressing the wild type *CLRN1* minigene. Analogous to the results obtained from HEK293 cells, one of these bands originates from the usage of an alternative splice donor site in the aberrant exon and corresponds to one of the annotated, non-protein-coding *CLRN1* splice isoforms (ENS000000485607.1). Other bands could be identified as hybrids composed of different combinations of correctly spliced, aberrantly spliced and alternatively spliced products (Suppl. Fig. 1D-F).

Finally, we also addressed potential off-targets of AON treatment using RNA-seq of HEK293 cells co-transfected with the mutant *CLRN1* minigene and A2.2. Cells expressing the mutant *CLRN1* minigene in the absence of AONs served as control. Overall, the correlation of the expression levels was high ($R^2 \sim 0.79$) with a slight decrease of basal expression levels in AON treated cells. Importantly, among the most changed transcripts (\log_2 fold change > 2) there was no enrichment for transcripts located on or near *in silico* predicted A2.2 binding sites (see Methods for details) (Suppl. Fig. 2E, F). However, we cannot exclude that some off-targets might be detectable under conditions which more accurately resemble the native situation, e.g. the retina of the patients. When co-expressing the *CLRN1* mutant minigene with A2.2, we detected four annotated *CLRN1* splice isoforms (Suppl. Fig. 2E). By contrast, in HEK293 cells

expressing the mutant minigene alone, we detected two of these isoforms, one of which was only weakly expressed in the A2.2 treated cells. These results further support the effectiveness of the A2.2 treatment on the correction of the mutant *CLRN1* mRNA splicing.

In conclusion, the use of AONs, particularly A2.2, achieved a substantial correction of aberrant splicing caused by the c.254-649T>G mutation. AONs therefore provide another possible strategy, in addition to the CRISPR-Cas9 approach, for treating USH3A patients carrying this mutation.

Combination of CRISPR-Cas9 and AONs in cells stably expressing the CLRN1 minigene

As CRISPR-Cas9 and AONs act on different levels, i.e. the genomic DNA and the pre-mRNA level, respectively, one would expect that combining these technologies would increase the splicing rescue efficiency. To test for a potential synergism of the two approaches, we generated HEK293 cell lines stably expressing the wild type or the mutant *CLRN1* minigene, which was randomly integrated into the host genome (Fig. 3A). In this setting, the *CLRN1*-specific Cas9/sgRNA complex can target both, the native and the transgenic *CLRN1* locus. Transfected HEK293 cells transiently expressing *CLRN1* minigenes were not used for this experiment because transfected plasmid DNA differs from native chromatin in the target cells. As the efficiency of CRISPR-Cas9 gene editing is known to depend on epigenetic factors, we decided to use cells stably expressing the *CLRN1* transgene.

Surprisingly, stable HEK293 cells co-transfected with the *SpCas9*- and sgRNAs-containing plasmid together with A2.2 resulted in a decreased enzymatic activity of *SpCas9*. This combination yielded significantly lower levels of cut DNA as opposed to cells expressing the *SpCas9*/sgRNA cassette alone or the *SpCas9*/sgRNA cassette in combination with a control AON targeting the rhodopsin locus (Fig. 3B). These results suggest that AONs inhibit the enzymatic activity of *SpCas9*, potentially by binding to the *CLRN1* locus at the genomic level. Since the binding position of the *CLRN1* sgRNAs and A2.2 do not overlap, this inhibition cannot be explained by a direct competitive effect of the AON and the sgRNAs, but rather by steric hindrance of the *SpCas9* enzyme preventing it from binding or cutting the DNA. In line with the

results obtained for the genomic level, a subsequent RT-PCR analysis from the same cells revealed no apparent synergistic effects of the combinatory approach on the *CLRN1* transcript (Fig. 3C). Notably, when the *SpCas9*/sgRNA cassette was expressed alone, the splicing correction efficiency ($45.92 \% \pm 1.24 \%$) was substantially higher than the DNA cutting efficiency ($26.8 \% \pm 3.22 \%$), suggesting that the actual gene editing efficiency is higher than the values measured by the densitometric analysis of the PCR bands from the genomic DNA. Collectively, we show that the combination of CRISPR-Cas9 and AONs has no synergistic effect on the correction of the splicing defect caused by the c.254-649T>G mutation, and provide the first evidence that AONs might act as locus-specific *SpCas9* inhibitors.

CRISPR-Cas9 gene editing in transfected ARPE-19 and transduced human RPE cells

It is well established that the efficiency of CRISPR-Cas9-mediated gene editing can be cell type dependent (20). In this regard, targeting cells which express *CLRN1* endogenously would be more therapeutically relevant. We therefore tested two different retinal pigment epithelium (RPE)-derived cell lines for *CLRN1* expression, i.e. ARPE-19 (21) and human retinal pigment epithelial (hRPE) cells provided by the LMU Eye Hospital Munich, Germany. Both cell lines expressed *CLRN1* at similar levels (Fig. 4A) suggesting that this gene might also be expressed in native RPE cells in the retina. We first transfected the *SpCas9*-T2A-EGFP construct in ARPE-19 cells and performed FAC-sorting of the GFP positive cells (Suppl. Fig. 3A). After analyzing the *CLRN1* locus, we obtained a gene editing efficiency comparable to transfected or sorted HEK293 cells ($19.05 \% \pm 0.77 \%$, Fig. 4B, C). Analogous to the results obtained from HEK293 cells shown in Suppl. Fig. 1A, B, sequencing of these bands revealed no obvious background signal in the electropherograms (Suppl. Fig. 3B, C).

To approximate a therapeutically applicable approach, we employed rAAVs (rAAV7m8) as gene therapy vectors. Due to their limited genome packaging capacity, the *SpCas9* and the sgRNAs would have to be co-delivered in two separate rAAV-vectors for *in vivo* applications. We therefore assessed whether our CRISPR-Cas9 approach could perform with similar effectiveness in a *CLRN1*-expressing cell line following dual rAAV co-transduction (Fig. 4D).

As the co-transduction efficiency of ARPE-19 cells with two titer-matched rAAVs expressing the *SpCas9* or the sgRNA cassette was very low (data not shown), we conducted the same experiment with hRPE cells. Upon transduction we could detect the *CLRN1* bands expected to occur after *SpCas9*-mediated editing of the corresponding locus. Quantification of *CLRN1* editing revealed that this process was more efficient than in HEK293 and in transfected ARPE-19 cells ($29.26 \% \pm 2.06 \%$, Fig. 4E, F). These results show that the endogenous *CLRN1* locus can be efficiently edited via CRISPR-Cas9, when delivered using a dual rAAV approach. In the corresponding electropherograms no background signal was observed (Suppl. Fig. 3D, E).

Quantification and off target-analysis of CRISPR-Cas9-mediated gene editing using NGS

So far, the efficiency of the CRISPR-Cas9 gene editing was calculated via the densitometric analyses of the bands obtained from the genomic DNA of respective cell lines. As this semi-quantitative approach might not reliably reflect the actual gene editing efficiency, we carried out targeted next generation sequencing (NGS) of the PCR products amplified from the genomic DNA of two FAC-sorted cell lines transiently expressing the *SpCas9*-T2A-EGFP/sgRNA complex, i.e. HEK293 and ARPE-19 cells. The gene editing efficiency for both cell lines was substantially higher compared to the semi-quantitative densitometric calculations (84.3 % for HEK293 cells and 63.9 % for ARPE-19 cells) (Suppl. Fig. 4A-C). The molecular explanation for this discrepancy remains unclear, however, it suggests that the gene editing efficiency calculation requires elaborate analyses to be determined more accurately, e.g. by single cell sequencing, usage of unique molecular identifiers or by PCR-free methods. Moreover, the NGS analysis revealed that in both cell types for the vast majority of cases the sequence between the sgRNA target sites was removed as expected (44 – 47 %, Suppl. Fig. 4D). In this context, we also identified some edited sequences with lower frequencies, which contained additional small insertions or deletions at the cut site. However, in all of these cases the potential mutation-containing sequence was successfully removed from the intron. From this it can be concluded that irrespective of the cell type the majority of sgRNA cutting events results the desired DNA modification.

It is also conceivable that our CRISPR-Cas9 approach might cause off-targets at the genome level. To address this issue, we performed whole exome sequencing (WES) using DNA from FAC-sorted HEK293 cells transfected with the SpCas9-T2A-EGFP/sgRNA complex. Importantly, no off-targets were detected under these conditions (Suppl. Fig. 4E). Using this approach, we could also confirm the deletion of the region flanking the c.254-649T>G mutation caused by SpCas9 cleavage (Suppl. Fig 4F). We cannot exclude that off-targets might occur in other non-coding (regulatory) regions which cannot be covered by this strategy. This requires a whole genome sequencing approach, which is out of scope of this study, but could be conducted in appropriate cell lines in a more advanced preclinical setting.

AONs for splicing correction in the retina

The evaluation of the CRISPR-Cas9 gene editing is more challenging *in vivo* and would require the generation of humanized *CLRN1* mouse models. Delivering the *CLRN1* minigene via rAAVs *in vivo* would not reflect the conditions required for CRISPR-Cas9 genomic *CLRN1* editing as the rAAV genome resides in the nucleus as an episomal state. However, as AONs act at the transcript level, we tested whether the AON-approach would result in correction of the splice defect caused by the c.254-649T>G *CLRN1* mutation *in vivo*. For this purpose, we used rAAV-mediated gene delivery to express the wild type or mutant human *CLRN1* minigenes in the mouse retina. To ensure correct localization, the *CLRN1* minigene was expressed under the murine rhodopsin promoter (Fig. 5A). The rAAVs were subretinally injected into wildtype C57BL/6J mice alone or co-delivered with A2.2 (Fig. 5B). Four weeks after co-delivery, we extracted RNA from the injected retinas and analyzed the mRNA splicing of the *CLRN1* minigene via RT-PCR. Importantly, when comparing wild type and mutant *CLRN1* minigene-born transcript in absence of A2.2, we could confirm the splice defect of the c.254-649T>G mutation (Fig. 5C). In line with the *in vitro* experiments, the presence of the additional two bands above the regularly spliced *CLRN1* was detected for wild type *CLRN1* in the retina. Co-delivery of A2.2 with the mutant *CLRN1* minigene resulted in a significantly

increased percentage of correctly spliced *CLRN1*, when compared to the mutant *CLRN1* minigene alone (29.73 % \pm 2.62 % vs. 13.48 % \pm 0.59 %) (Fig. 5D).

Taken together, we could confirm the mRNA splicing defect of the c.254-649T>G *CLRN1* mutation under a close-to-native setting and show a significant splicing rescue upon co-delivery of A2.2.

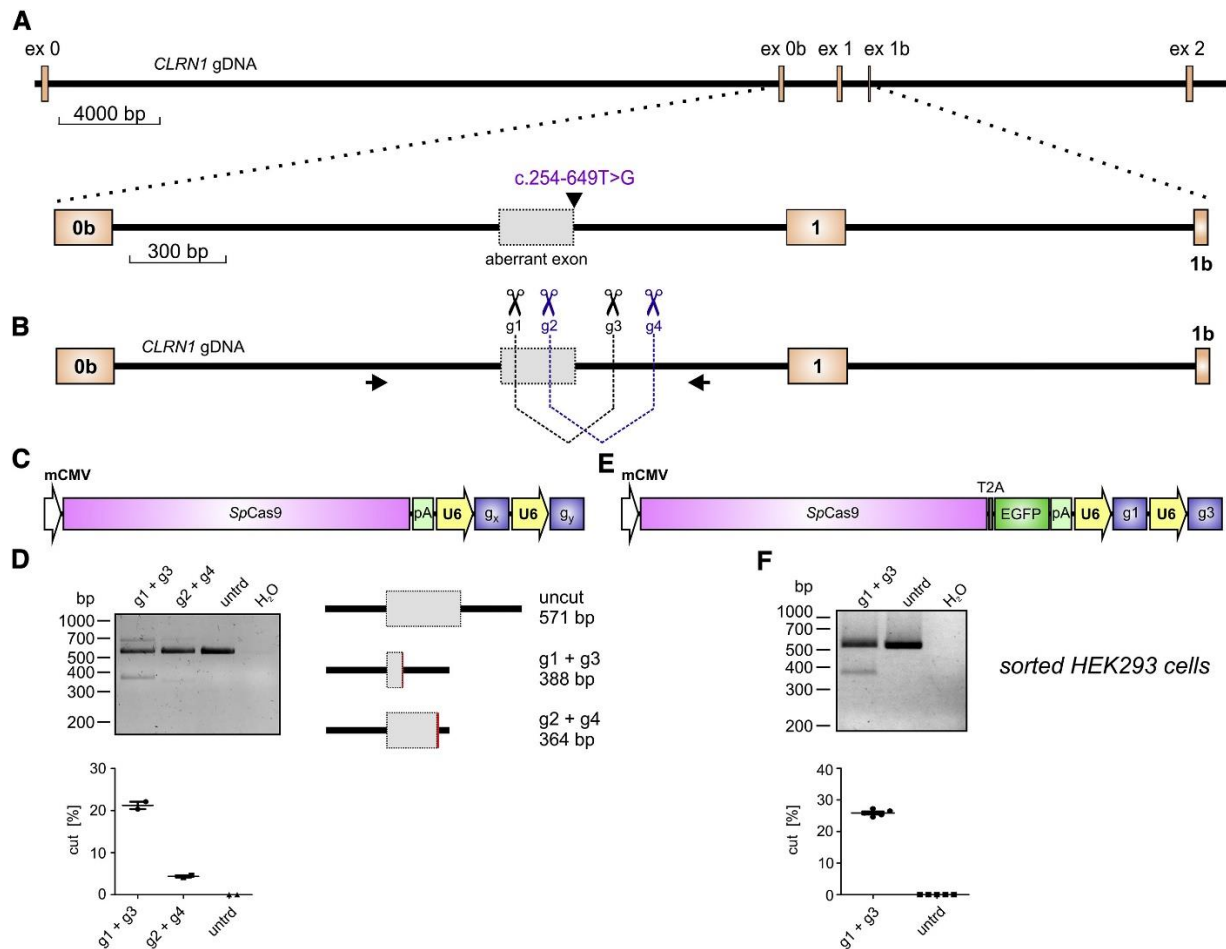


Fig. 1 CRISPR-Cas9-mediated *CLRN1* editing. A, Upper panel, True to scale representation of the *CLRN1* gene encompassing exons 0 – 2. gDNA, genomic DNA. Lower panel, The c.254-649T>G mutation generates an aberrant exon in intron 0b. B, Binding positions of *CLRN1* sgRNAs (g1 – g4) and primers used for amplification of genomic DNA via PCR displayed in D and F. C, *SpCas9* expression cassette used for the transfection of the cells shown in D. g_x and g_y , single guide RNA combinations (g1 + g3 or g2 + g4). mCMV, minimal CMV promoter. D, Upper panel, PCR amplifying the endogenous wild type *CLRN1* locus from genomic DNA originating from HEK293 cells transiently expressing the *SpCas9* with two combinations of sgRNAs as indicated. Lower panel, Semi-quantitative densitometric analysis of the DNA editing efficiency for the single combinations and untreated (untrd) cells. E, *SpCas9*-cassette used for the transfection of the cells shown in F. F, PCR amplifying the endogenous wild type *SpCas9* with the g1 + g3 combination. Lower panel, Semi-quantitative densitometric analysis of the results shown in the upper panel.

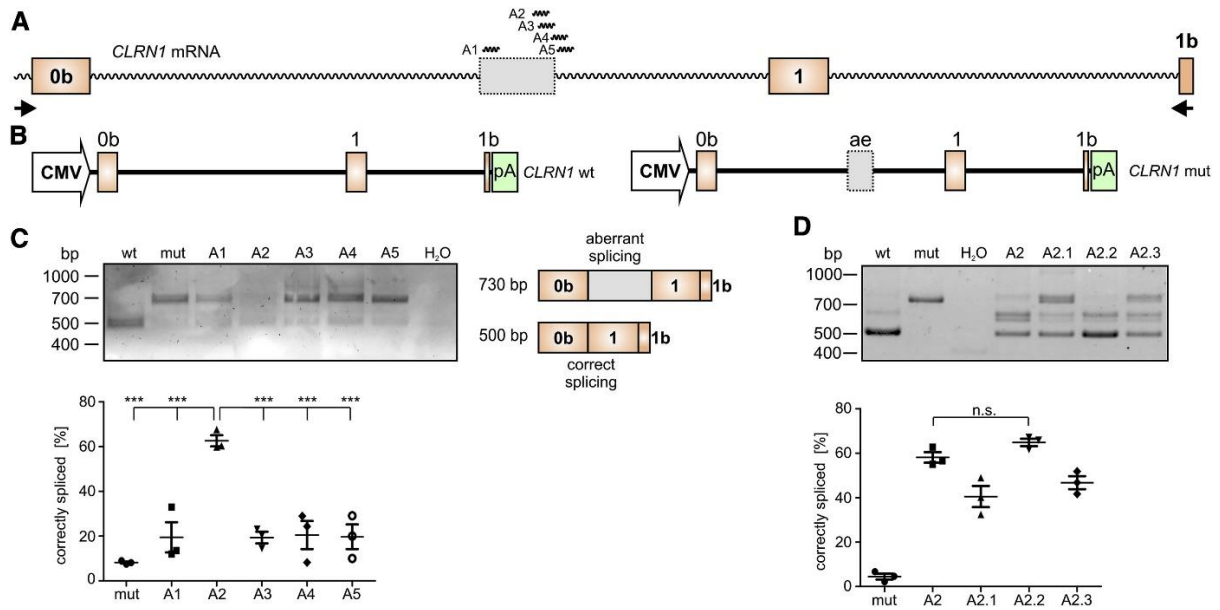


Fig. 2 AON-mediated correction of *CLRN1* mRNA splicing. A, Binding positions of *CLRN1* AONs (A1 – A5) used for initial screening. Primers used for RT-PCR in C and D are shown as arrows. B, Wild type (wt, left) and mutant (mut, right) *CLRN1* minigene expression cassettes used for the transfection of the cells shown in C and D. C, RT-PCR from HEK293 cells transiently expressing the *CLRN1* minigene in combination with the single AONs as indicated. The corresponding semi-quantitative densitometric analysis is displayed below. D, RT-PCR from HEK293 cells transiently expressing wt or mut *CLRN1* minigenes in combination with different modified versions of A2 (cf. Suppl. Table 1). n.s., not significant. Statistical analysis was performed with a one-way ANOVA and Bonferroni's post-hoc test, *, $p \leq 0.05$; **, $p \leq 0.01$; ***, $p \leq 0.001$, $n = 3$.

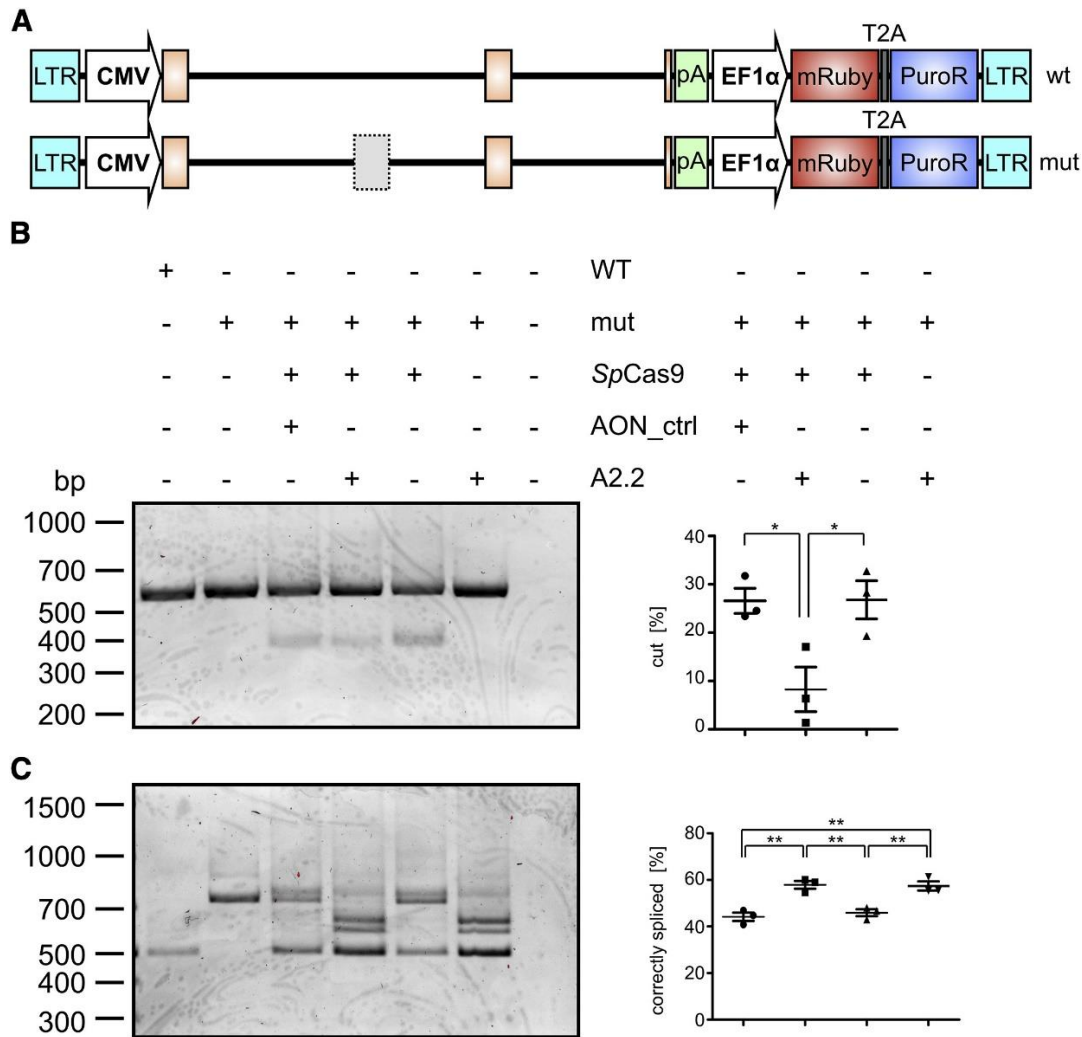


Fig. 3 Combination of AONs and CRISPR-Cas9 in a stable cell line expressing the *CLRN1* minigene. A, wt or mut *CLRN1* DNA cassettes used for the generation of the stable HEK293 cell lines. LTR, long terminal repeat. CMV, cytomegalovirus promoter. pA, polyadenylation signal. EF1 α , human elongation factor 1 alpha promoter. PuroR, pyromycine resistance gene. B, Left panel, PCR from genomic DNA isolated from wt or mutant stable cell lines. The mutant cell lines were (co)-transfected with the *SpCas9* and sgRNAs containing expression cassette and AONs as indicated. AON_ctrl, control AON targeting the rhodopsin (*RHO*) locus. Right panel, semi-quantitative analysis of the PCR band intensities for the three relevant combinations shown left. C, Left panel, RT-PCR from the same cells and the same combinations as shown in B. Right panel, semi-quantitative analysis of the PCR band intensities for the four relevant combinations shown left. Statistical analysis was done with a one-way ANOVA and Bonferroni's post-hoc test, *, $p \leq 0.05$; **, $p \leq 0.01$; ***, $p \leq 0.001$, $n = 3$.

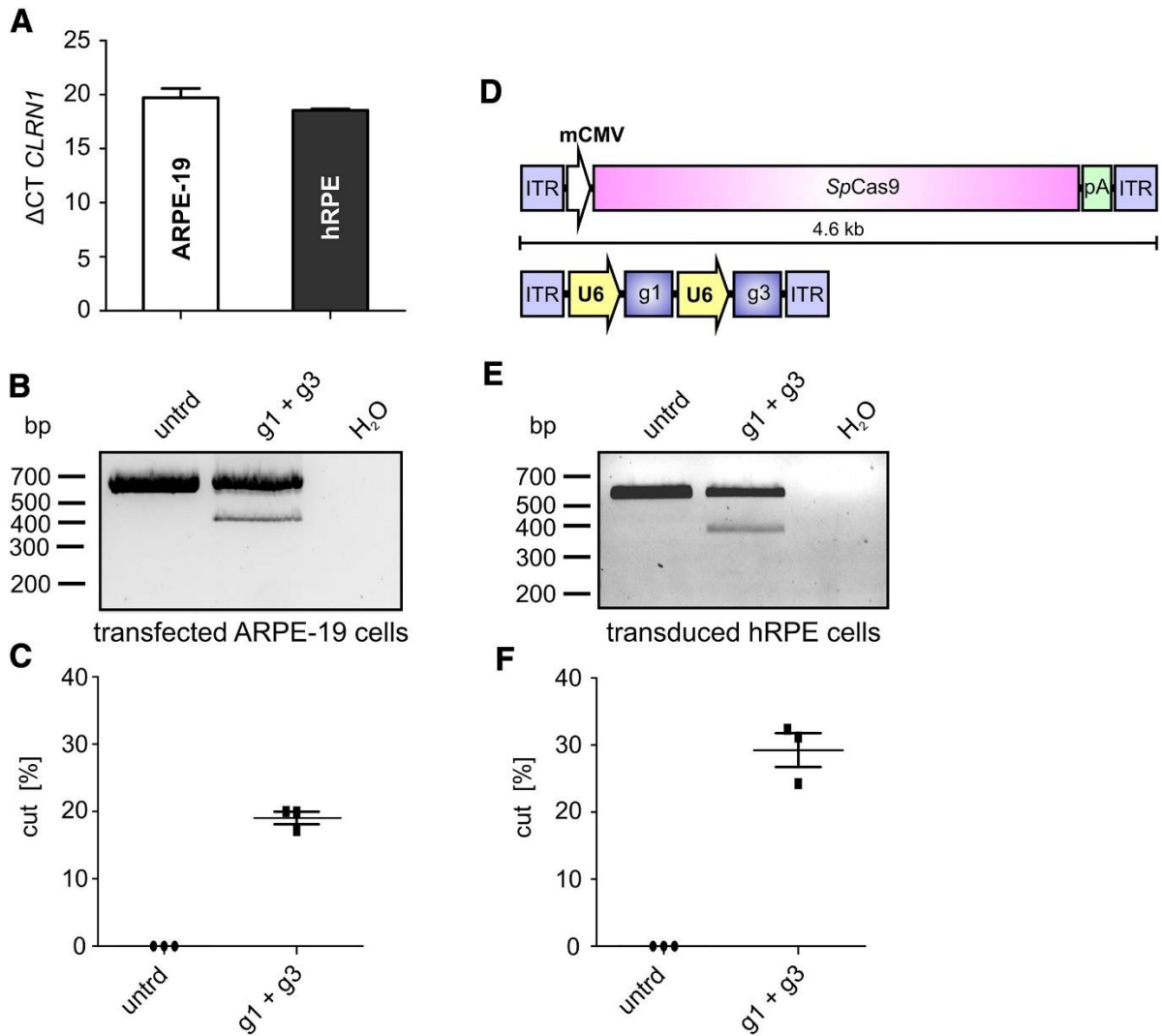


Fig. 4 CRISPR-Cas9-mediated *CLRN1* gene editing in transfected ARPE-19 and rAAV-transduced human RPE cells. A, *CLRN1* expression in ARPE-19 and hRPE cells. ΔCT , cycle threshold of the *CLRN1* expression normalized to beta actin (*ACTB*). B, PCR of genomic DNA isolated from transfected and FAC-sorted ARPE-19 cells. untrd, untreated. C, Densitometric analysis of the PCR band intensities shown in B. D, rAAV expression cassette used for transduction of hRPE cells. ITR, inverted terminal repeats. E, PCR from genomic DNA isolated from transduced hRPE cells one week post-transduction. F, Densitometric analysis of the PCR band intensities shown in E. Statistical analysis was performed using the Student's t-test, $n = 3$.

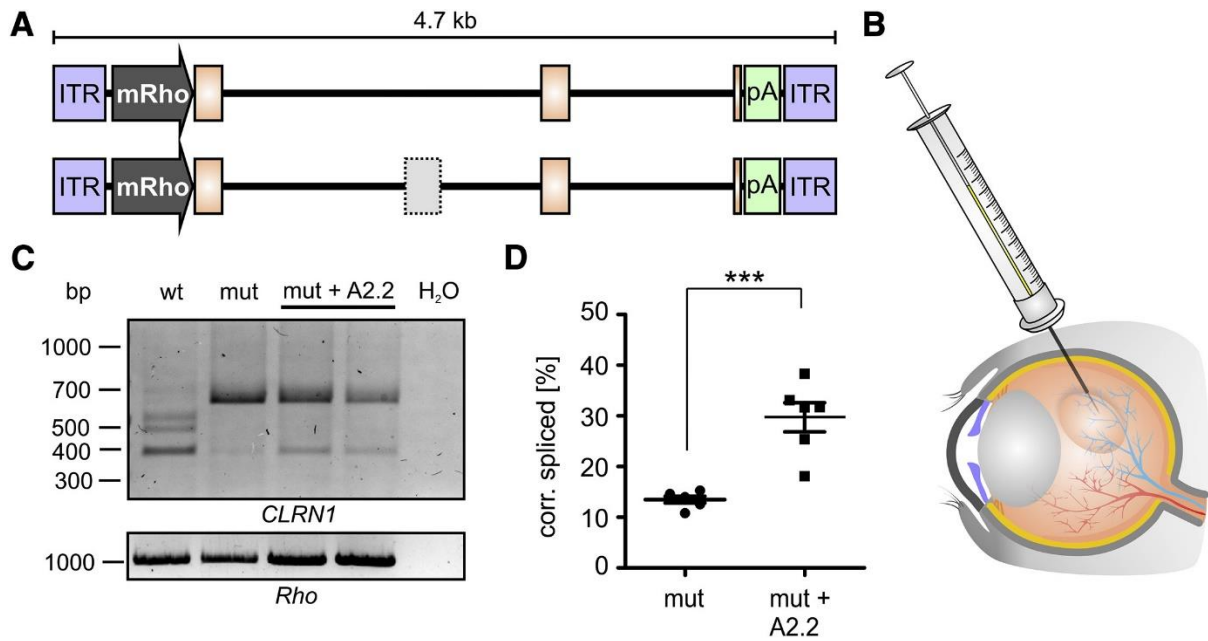


Fig. 5 AON-mediated *CLRN1* c.254-649T>G splice rescue in injected retinas. A, wt and mut *CLRN1* minigene containing rAAV cassettes used for subretinal injections. ITR, inverted terminal repeats. mRho, mouse rhodopsin promoter. B, rAAVs in presence or absence of naked A2.2 were subretinally injected to wild type C57BL/6J mice. C, RT-PCR from retinas of injected mice four weeks post-injection. Two retinas from two different mice were pooled for each RT-PCR experiment. *Rho* expression served as a control. C, Semi-quantitative analysis of the PCR band intensities for the single combinations as indicated. Statistical analysis was performed using the Student's t-test. *, $p \leq 0.05$; **, $p \leq 0.01$; ***, $p \leq 0.001$, $n = 6$.

Discussion

In this study, we evaluate for the first time the potential of CRISPR-Cas9 and AONs as single or as combinatory approaches to rescue the splice defect caused by a deep intronic c.254-649T>G *CLRN1* mutation. Both approaches were tested in different human cell lines and yielded reasonable splice rescue efficiency. A similar CRISPR-Cas9 approach has been used in the past for treatment of deep intronic splicing mutations found in the *CEP290* gene causing Leber congenital amaurosis (LCA) (22). AONs have also been utilized in the past for treatment of splicing mutations in several genes associated with retinal disorders, e.g. LCA, Usher syndrome type II or Stargardt disease (23-25). Moreover, both, CRISPR-Cas9 and AONs, have been FDA-approved for first clinical trials to treat LCA patients carrying the most common deep intronic variant in *CEP290*, i.e. c.2991+1655A>G (26, 27). This outlines the great potential of these technologies for future gene therapies. Here, we provide promising results which could represent initial steps towards the first clinical trial for USH3A patients using one of these technologies.

AONs can be delivered intravitreally (or subretinally) as naked molecules expected to distribute evenly across the retina and to be taken up by the different retinal cell types. AONs are also conveniently produced, which circumvents the elaborate and costly process of rAAV production. However, AON-based treatment requires a continuous administration (typically every few months) via subretinal or intravitreal injection. This increases the risk of injection-mediated comorbidities and decreases the patients' compliance. In contrast, CRISPR-Cas9-based approaches typically require only a single treatment. The most widely used and best characterized Cas9 subtype is *SpCas9*, derived from *Streptococcus pyogenes*. *SpCas9* can be efficiently expressed in all retinal cells utilizing rAAV vectors carrying e.g. the ubiquitous minimal CMV promoter (22). Due to the payload limit of rAAVs (approx. 4.7 kb), the *SpCas9* cannot be packaged together with the corresponding sgRNA cassette and therefore needs to be delivered via two separate rAAVs. It has been shown that co-application of dual rAAVs into the retina results in sufficient transduction levels, which render its therapeutic implementation feasible (18, 22, 28, 29). Furthermore, to combat the potential risk of immune responses due

to the expression of the bacterial *SpCas9* enzyme, strategies have been developed to ensure only a transient expression of this protein in the target cells (22). Moreover, it remains to be determined what percentage of wild type *CLRN1* transcript is sufficient to achieve a therapeutic effect in the USH3A patients and/or animal models. It has been shown for other retinal and non-retinal autosomal-recessive disorders that already a few percent of the intact gene can achieve substantial functional and phenotypic rescue (30-32). Our gene editing efficiency ranges between approx. 30 % obtained via densitometric analysis and 64 – 84 % as calculated from the NGS data. The exact reason for this discrepancy between the methods remains unknown. But regardless of which of these values most closely reflects the true efficiency of gene editing, it may already be high enough to achieve therapeutic success in patients.

We provide primary evidence that both, the CRISPR-Cas9 and the AON approach, do not cause off-targets under the conditions used herein further supporting the therapeutic potential of these strategies. Nevertheless, additional experiments are required to interrogate off-target effects in a broader and clinically more relevant setting using e.g. whole genome sequencing or similar quantitative approaches. A recent study reported no apparent off-targets for two sgRNAs in a CRISPR-Cas9-based approach for LCA treatment in the retina (22). This shifts the risk-benefit balance in favor of utilizing such gene editing technologies to treat conditions for which other alternatives are currently unavailable.

One plausible strategy to increase the splice rescue efficiency and thus the chance of a successful treatment would be to combine both technologies in a single approach. Our results, however, suggest that AONs, which target similar positions close to the sgRNA target sites, reduce the *SpCas9*-mediated DNA cleavage efficiency. In line with other studies (33, 34), this indicates that AONs can also efficiently target genomic DNA and raises the question whether combining CRISPR-Cas9 and AONs is meaningful. This finding is particularly important as it provides a new research avenue for developing AON-based and target-specific *SpCas9* inhibitors.

This work evaluates the therapeutic potential of CRISPR-Cas9- and AON-based strategies to correct the splicing of the *CLRN1* c.254-649T>G mutation, and offers initial premise for further preclinical development, which could lead to the first clinical trials for USH3A patients.

Materials and Methods

Animals

For all animal experiments in this study, wild type C57BL/6J mice were used. All procedures involving animals were performed with permission of the local authorities (District Government of Upper Bavaria) and German laws on animal welfare (Tierschutzgesetz). Anesthesia was performed by intraperitoneal injection of ketamine (40 mg/kg body weight) and xylazine (20 mg/kg body weight). Euthanasia was performed by isoflurane and cervical dislocation.

Construction and cloning of expression plasmids

Minigenes suitable for splicing analysis were constructed and cloned as described previously (7, 35). The wild type (wt) and mutant (mut) *CLRN1* minigenes were synthesized by BioCat (Heidelberg, Germany) and delivered in a pcDNA3.1 standard vector. These constructs were used for transient expression in HEK293 cells. For a stable expression in this cell line, the wt and mut minigene cassettes including the SV40 polyadenylation signal were subcloned into a piggybac vector (PB514B-2-SBI, BioCat, Heidelberg, Germany). For expression in mouse photoreceptors, the *CLRN1* wt and mut minigenes were subcloned into the pAAV2.1 vector (36) equipped with a murine rhodopsin promoter. The *SpCas9* coding sequence and short synthetic polyadenylation signal was taken from the PX551 plasmid (37) and subcloned into the pAAV2.1 plasmid containing a minimal CMV promoter. PX551 was a gift from Feng Zhang (Addgene plasmid #60957; <http://n2t.net/addgene:60957>; RRID: Addgene_60957). Due to the limited rAAV packaging capacity of approximately 4.7 kb, the different sgRNA sequences (Suppl. Table 2) driven by a U6 promoter were cloned into a separate pAAV2.1 plasmid. For FACS experiments, a T2A and EGFP sequence was added 3' of the *SpCas9* coding sequence and the sgRNA expression cassettes were cloned into the same expression vector. All constructs were sequenced prior to use (Eurofins Genomics, Ebersberg, Germany).

Cell culture and transfection

The ARPE-19 cell line was a gift from the LMU University Eye Hospital in Munich, Germany. The cells were cultivated in DMEM/F-12 (1:1) medium (Gibco™, Thermo Fisher Scientific, Waltham, MA) containing L-Glutamine, 10 % FBS (Biochrom, Merck, Darmstadt, Germany) and 1 % penicillin/streptomycin (Biochrom, Merck) at 37 °C and 5 % CO₂. The cells were transfected with a SpCas9- and sgRNAs-containing plasmid using the standard calcium phosphate transfection protocol. For this purpose, cells were seeded onto 6 cm cell culture plates and incubated overnight until they reached the desired confluence of approximately 70 %. For the transfection, 6 µg of plasmid DNA (3 µg per plasmid) were mixed with 30 µl of 2.5 M CaCl₂ and 270 µl H₂O. 600 µl 2x BBS were added dropwise during vortexing. The transfection mix was incubated for 3 – 4 minutes at room temperature and added dropwise to the culture medium. The cells were incubated in a 5 % CO₂ setting for 3 – 4 h, the culture medium was replaced and the cells were maintained at 10 % CO₂ for approximately 48 h. No transfection toxicity was detected. The murine 661W cell line derived from retinal tumors was kindly provided by Dr. Muayyad Al-Ubaidi, University of Houston (38). The cells were cultured in DMEM GlutaMAX medium (Thermo Fisher Scientific, Waltham, MA) supplemented with 10 % FBS (Biochrom, Merck) and 1 % Anti-Anti (Thermo Fisher Scientific, Waltham, MA) at 37 °C and 10 % CO₂. Immortalized mouse embryonic fibroblasts (MEFs) were generated as previously described (39, 40). MEF cells were cultured in DMEM GlutaMAX medium supplemented with 10 % FBS (Biochrom, Merck) and 1 % penicillin/streptomycin (Biochrom, Merck) at 37 °C and 5 % CO₂. Transient transfections of 661W and MEF cells were performed using the TurboFect transfection reagent (Invitrogen, Thermo Fisher Scientific, Waltham, MA) according to the manufacturer's instructions. HEK293 cells were transfected with the respective minigenes and (if applicable) with a SpCas9/sgRNA-encoding plasmid using the TurboFect transfection reagent (Invitrogen, Thermo Fisher Scientific, Waltham, MA).

RT-PCR

48 h post-transfection, the cells were harvested and lysed using the mixer mill MM400 (Retsch, Haan, Germany). RNA was isolated using the RNeasy Mini Kit (QIAGEN, Hilden, Germany) according to the manufacturer's instructions and RNA concentration purity was determined via the NanoDrop2000 (Thermo Scientific, Waltham, MA). cDNA was synthesized using the RevertAid First Strand cDNA Synthesis Kit (Thermo Fisher Scientific, Waltham, MA) according to the manufacturer's instructions for 1 µg total RNA. For subsequent RT-PCR, the Herculase II fusion DNA polymerase (Agilent Technologies, Santa Clara, CA) was used according to the manufacturer's instructions using appropriate primers designed to exclusively amplify the CLRN1 minigene-born transcript (Suppl. Table 3). The PCR products representing the differentially spliced transcripts were isolated using the QIAquick Gel Extraction kit (Qiagen, Venlo, Netherlands) and sequenced (Eurofins Genomics, Ebersberg, Germany).

Isolation of genomic DNA and PCR

Genomic DNA (gDNA) was isolated from transfected and untreated cells. The cells were lysed in RLT buffer (Qiagen, Venlo, Netherlands) containing 1 % β-mercaptoethanol (Sigma Aldrich, St. Louis, MO) using the mixer mill MM400 (Retsch, Haan, Germany). For gDNA isolation, the lysate was loaded onto a Zymo-Spin IIC-XL DNA column (Zymo Research, Irvine, CA). The column was subsequently washed once using 600 µl of the DNA Pre-Wash Buffer (Zymo Research, Irvine, CA) followed by two washing steps with 600 µl of the g-DNA Wash Buffer (Zymo Research, Irvine, CA). Genomic DNA was eluted in the appropriate volume of H₂O containing 20 mM 2,6-di-tert-butyl-4-methylphenol. For subsequent PCR using the Q5 polymerase according to the manufacturer's instructions, 100 ng of gDNA were used. All obtained PCR bands were isolated using the QIAquick Gel Extraction kit (Qiagen, Venlo, Netherlands) and sequenced (Eurofins Genomics, Ebersberg, Germany).

Fluorescence-activated cell sorting

HEK293 and ARPE-19 cells transfected with the *SpCas9*-T2A-EGFP construct were sorted via fluorescence-activated cell sorting (FACS) for nascent GFP. For this purpose, the cells were detached 48 h post-transfection using TryPLE. After detachment, the TryPLE was removed by centrifugation at 0.3 rcf for 5 min and aspirated. The cell pellet was resuspended in sample buffer (2 % FBS, 2 mM EDTA, 25 mM HEPES in PBS) and the suspension was stained with a viability dye (Sytox Blue, Thermo Fisher Scientific, Waltham, MA). Cell sorting was performed on a FACS Aria IIIu (Becton Dickinson, Franklin Lakes, NJ) equipped with the BD FACSDiva software v8.0. HEK293 and ARPE-19 cells were sorted with a 100 μ m nozzle at 20 psi and with a 130 μ m nozzle at 10 psi, respectively. Viable cells were gated from non-viable and from mock-transfected cells expressing the *SpCas9* without any fluorophore. A range between 100,000 – 250,000 cells were sorted. GFP-expressing cells were sorted into RLT buffer containing 1 % β -mercaptoethanol (Sigma Aldrich, St. Louis, MO) and used directly for gDNA extraction.

Whole exome sequencing and off-target analysis

1 μ g of gDNA of native HEK293 and *SpCas9*-treated cells was fragmented to an average size of 150 bp using the Covaris M220 Focused-ultra sonicator (Covaris, Woburn, MA). After DNA repair with the NEBNext FFBE DNA repair mix (New England Biolabs Inc., MA) paired-end sequencing libraries were constructed using the SureSelectXT reagent kit (Agilent, Santa Clara, CA). End repair, adapter ligation, and PCR enrichment and was carried out according to the manufacturer's instructions. Protein-coding sequences were captured using SureSelect Human All Exon V6 (Agilent, Santa Clara, CA) according to the manufacturer's instructions. Exome libraries were sequenced paired-end on an Illumina HiSeq 1500 sequencer with a read length of 100 nucleotides to an average coverage of 50x. The reads were mapped to the human reference genome (hg19) with BWA-MEM (41) using default settings. Single-nucleotide polymorphisms and INDELS were analyzed following the GATK workflow to discover somatic short variants (SNVs + Indels) (42, 43). Within the workflow, *Mutect2* from the *GATK Analysis*

Toolkit was used to obtain variants specific to *SpCas9*-treated cells. The obtained variants were filtered using *FilterMutectCalls*, resulting in 273 SNVs and 35 Indels passing the filter (FILTER: PASS). Off-target analysis of those variants was performed by calculating the minimum Levenshtein distances. The two guide RNAs [5'-AAATCTGGCAGGACCAATCTTGG and 5'-TTAATGTAGCACAAAGCTGTGGG] were aligned in a sliding window, starting 30 bp up- and downstream of each variant position and the alignment with the smallest Levenshtein distance was determined. An alignment was only taken into consideration if the PAM sequence (NGG) was present. For comparison, the approach was applied to 1,000 randomly selected genomic positions.

mRNA pre-processing and sequencing

For mRNA-seq library production, we ran a scaled-up version of the SMARTseq2 protocol (44). Briefly, from 100 ng of total RNA, mRNA was captured with a mix of 0.5 µl of 20 µM oligo dT primer and 0.5 µl of 20 mM dNTPs followed by heating to 72° C for 3 min and immediately putting it into an ice-water bath. Next, in a 10 µl reaction, double stranded cDNA was generated by adding 2 µl of 5x Superscript II first-strand buffer (Thermo Fisher Scientific, Waltham, MA), 2 µl of 5 M Betaine, 0.6 µl of 100 mM MgCl₂, 0.5 µl of 100 mM DTT, 0.4 µl of RNasin (Promega, Madison, WI), 0.5 µl of 20 µM of template-switch oligo (20 µM) and 0.5 µl of SuperScript II reverse transcriptase (200 U/µl, Thermo Scientific, Waltham, MA) and incubating the solution for 90 min at 42° C, followed by 14 cycles (50° C for 2 min, 42° C for 2 min) and heat inactivation (70° C for 15 min). Pre-amplification was done by addition of 12.5 µl of 2x KAPA HiFi HotStart Ready mix, 0.25 µl of 10 µM IS PCR primers and 2.25 µl of nuclease-free water in a thermos protocol of 98° C for 3 min, 10 pre-amp cycles (98° C for 20 sec, 67° C for 15 sec, 72° C for 6 min), followed by 5 min at 72° C and hold at 4° C. Purification was done with AMPure XP beads (Beckman Coulter, Brea, CA), cDNA was quantified with Qubit (Thermo Scientific, Waltham, MA) and checked for fragment length distribution on an Agilent Bioanalyzer chip (Agilent, Santa Clara, CA). Next, 7 ng of cDNA were fragmented in a 20 µl reaction by incubation with 1 µl of Tn5 enzyme from the Illumina Nextera library preparation kit (Illumina, San Diego, CA)

and 10 µl of 2x tagmentation DNA buffer for 10 min at 55° C. Tagmented cDNA was purified with MinElute columns (Qiagen, Venlo, Netherlands) and PCR amplified with NEBNext High-Fidelity 2x PCR Mastermix, 1 µl of each 10 µM Nextera index 1 and Nextera index 2 primer (Illumina, San Diego, CA) with a thermos protocol of 72° C for 5 min, 98° C for 30 sec, 7 cycles (98° C for 10 sec, 63° C for 30 sec, 72° C for 1 min), 72° C for 5 min and hold at 4° C. The final library was purified with AMPure beads, quantified by Qubit and sequenced for 100 basepairs using a V3 single read flow cell on a HiSeq 2500 (Illumina, San Diego, CA). The generated data was trimmed for quality and adapter reads with TrimGalore! (https://www.bioinformatics.babraham.ac.uk/projects/trim_galore/) and mapped with the STAR aligner (45). Duplicates were marked with the MarkDuplicates function from Picard tools (<https://broadinstitute.github.io/picard/>) and the reads were summarized with RSEM (46).

AON off-target analysis

In silico prediction for genomic binding sites was performed with gggenome online tool (<https://gggenome.dbcls.jp/hg38/4/>) using the AON sequence (5'-CUUUCAUCUGGUGAGGCAUCAGC-3') to query the human genome (top and bottom strand and allowing up to 4 mismatches/gaps). Potential binding sites (n = 1150) were extended by 10 kb up- and downstream and all annotated transcript isoforms overlapping these windows were flagged as potential AON off-targets. Among the most deregulated transcripts (TPM log2 fold change > 1 or < -1) we found no enrichment for potential AON off-target transcripts by using a Fisher's exact test.

Targeted NGS and data processing

The 100 ng of the DNA isolated from FAC-sorted HEK293 and ARPE-19 cells were amplified using the Q5 polymerase (New England Biolabs, Ipswich, MA) according to the manufacturer's instructions (35 cycles) with appropriate primers (Suppl. Table 3). The PCR products were co-purified using the QIAquick Gel Extraction kit (Qiagen, Venlo, Netherlands). Purified amplicons from each sample were tagged with a unique NGS

barcode by PCR (7 cycles) followed by a final clean-up (Agencourt AMPure XP Beads, Beckman Coulter, Brea, CA). Finally, all samples (set to 10 nM) were pooled, loaded on an Illumina MiSeq sequencing machine (Illumina, San Diego, CA) and sequenced for 2x 250 bp paired-end with a MiSeq reagent kit V3 (Illumina, San Diego, CA) to approx. 200k fold coverage. The raw data was quality checked using FastQC and trimmed for adaptors or low-quality bases using the tools cutadapt and Trim Galore! (https://www.bioinformatics.babraham.ac.uk/projects/trim_galore/). Next, reads were sorted in a two-step procedure by (i) the NGS barcode adaptors to assign the reads and (ii) the first and the last 20 bp of each read to assign an amplicon ID. Obtained reads were then counted depending on the presence of either the original wild type sequence (at both sgRNA cutting sites plus/minus 15 bp) or the presence of a new fusion omitting a 187 bp fragment between the two sgRNA binding sites (see Suppl. Fig. 4).

Generation and delivery of antisense oligonucleotides

The sequence of the aberrant *CLRN1* exon was screened for exonic splicing enhancer (ESE) sequences using the ESEfinder 3.0 (<http://krainer01.cshl.edu/cgi-bin/tools/ESE3/ese finder.cgi?process=home>). AONs were designed to either cover multiple SRSF1, SRSF2, SRSF5 and SRSF6 motifs, the donor splice site or intronic splice enhancer motifs present in the intronic sequence adjacent to the novel donor splice site (Suppl. Table 1). All AON sequences contain 2'-O-methyl modified riboses and a phosphorothioate backbone and were synthesized by Eurofins Genomics (Ebersberg, Germany). For splicing rescue in transfected HEK293, 661W or MEF cells and in HEK293 stable cell lines, AONs were added to the cell medium at a final concentration of 250 nM (1.2 – 8 µg depending on the growth medium volume) unless stated otherwise. For *in vivo* experiments, AONs were suspended in the rAAV virus solution at a final concentration of 27.6 µg/µl.

Generation of stable cell lines

The stable cell lines were generated using the piggybac transposon system. Briefly, HEK293 cells were co-transfected with the respective *CLRN1* minigene containing piggybac vector and a piggybac transposase expression vector using a standard calcium phosphate transfection protocol. 24 h post-transfection, cells were selected for successful integration of the piggybac expression cassette by adding 2 µg/ml puromycin to the media for 8 days. The presence of RFP fluorescence indicating successful integration was confirmed using the EVOS® FL cell imaging system (Life Technologies, Thermo Fisher Scientific, Waltham, MA).

rAAV production

For the production of recombinant adeno-associated viral (rAAV) vectors, the 7M8 capsid (47, 48) was used for SpCas9 and sgRNA expression in human retinal pigment epithelial (hRPE) cells. For the expression of human *CLRN1* minigenes in the mouse retina, the 2/8YF capsid variant was used (49). rAAVs were produced as described previously (28, 50).

Human retinal pigment epithelium cell culture and transduction

The hRPE cells were a gift from the LMU University Eye Hospital in Munich, Germany. The cells were cultivated in DMEM GlutaMAX high glucose (4.5 g/l) medium (Gibco™, Thermo Fisher Scientific, Waltham, MA) containing 10 % FBS (Biochrom, Merck, Darmstadt, Germany) and 1 % penicillin/streptomycin (Biochrom, Merck, Darmstadt, Germany) at 37 °C and 5 % CO₂. The cells were transduced with 7M8 rAAVs with a multiplicity of infection (MOI) of 100,000. The medium was replaced after 48 h and cells were harvested 7 days post-transduction.

Subretinal injections and RT-PCR

1 µl containing 10¹⁰ viral particles and 27.6 µg of AON2.2 were delivered subretinally via a single injection into six-month old C57Bl/6J wildtype mice. Correct subretinal application was confirmed by transient retinal detachment during the injection. Four weeks post-

injection, the retinas were harvested and further processed for RNA isolation. Two retinas were pooled per construct. RNA isolation and cDNA synthesis were performed as described above. For cDNA synthesis, 1 µg total RNA was used. For RT-PCR, the Q5 polymerase (New England Biolabs, Ipswich, MA) was used according to the manufacturer's instructions and minigene-specific primers were used to avoid amplification of endogenous *Cln1*.

Quantitative RT-PCR

qRT-PCR was performed on the StepOnePlus Real-Time PCR System (Applied Biosystems, Thermo Fisher Scientific, Waltham, MA) using the SYBR Select Master Mix (Applied Biosystems, Thermo Fisher Scientific, Waltham, MA) according to the manufacturer's instructions. The expression of *CLRN1* was normalized to the housekeeping gene beta actin (*ACTB*) to obtain the Δ CT value. A higher Δ CT value reflects a lower gene expression with respect to *ACTB*. For quantification of the different *CLRN1* minigene-born splice isoforms, the expression was normalized to *ACTB* and to the overall expression of the transfected plasmid to avoid artefacts due to potential differences in the transfection efficiency.

Statistics

All values are given as mean \pm SEM. The number of replicates (n) and the used statistical tests are indicated in each figure legend for each experiment.

Acknowledgements

We thank Berit Noack and Lisa Richter for the valuable technical support. We also thank Dr. Claudia Priglinger from the LMU Eye Hospital Munich, Germany, for the gift of the hRPE and the ARPE-19 cell lines. Moreover, we want to thank Dr. Muayyad Al-Ubaidi for the gift of the 661W cells. We also acknowledge the Core Facility Flow Cytometry at the Biomedical Center, Ludwig-Maximilians-Universität Munich, Germany, for providing cell sorting services.

This work was supported by the Forschung Contra Blindheit - Initiative Usher Syndrome e.V and by the Deutsche Forschungsgemeinschaft, SPP2127, BE 4830/2-1 (both to E.B.). The funders had no role in study design, data collection and analysis, decision to publish, or preparation of the manuscript.

Author Contributions

E.B. designed the study and E.B. and L.R. supervised the project with input from M.B., A.P., N.K. and L.R. performed most of the experiments including qRT-PCRs, generation of the stable cell line and rAAV production. S.B. and M.P. conducted the subretinal injections. G.G. performed the NGS and the RNA-seq experiment and analyzed the data. A.G. performed the whole exome sequencing and A.G. and H.B. analyzed the data. E.B. and L.R. wrote the manuscript with contributions from A.P., N.K., M.P. and M.B.. E.B., M.B., H.B. and J.W. acquired funding. E.B., L.R., N.K., M.B., A.P., M.P. and S.B. analyzed and discussed the data with input from all authors.

CONFLICTS OF INTEREST

The authors declare no competing interests.

References

1. Mathur P, Yang J. Usher syndrome: Hearing loss, retinal degeneration and associated abnormalities. *Biochim Biophys Acta*. 2015;1852(3):406-20.
2. Zallocchi M, Meehan DT, Delimont D, Askew C, Garige S, Gratton MA, Rothermund-Franklin CA, Cosgrove D. Localization and expression of clarin-1, the *Clrn1* gene product, in auditory hair cells and photoreceptors. *Hear Res*. 2009;255(1-2):109-20.
3. Xu L, Bolch SN, Santiago CP, Dyka FM, Akil O, Lobanova ES, Wang Y, Martemyanov KA, Hauswirth WW, Smith WC, Handa JT, Blackshaw S, Ash JD, Dinculescu A. Clarin-1 expression in adult mouse and human retina highlights a role of Muller glia in Usher syndrome. *J Pathol*. 2020;250(2):195-204.
4. Vastinsalo H, Jalkanen R, Dinculescu A, Isosomppi J, Geller S, Flannery JG, Hauswirth WW, Sankila EM. Alternative splice variants of the *USH3A* gene *Clarin 1* (*CLRN1*). *Eur J Hum Genet*. 2011;19(1):30-5.
5. Ness SL, Ben-Yosef T, Bar-Lev A, Madeo AC, Brewer CC, Avraham KB, Kornreich R, Desnick RJ, Willner JP, Friedman TB, Griffith AJ. Genetic homogeneity and phenotypic variability among Ashkenazi Jews with Usher syndrome type III. *J Med Genet*. 2003;40(10):767-72.
6. Sankila EM, Pakarinen L, Kaariainen H, Aittomaki K, Karjalainen S, Sistonen P, de la Chapelle A. Assignment of an Usher syndrome type III (*USH3*) gene to chromosome 3q. *Hum Mol Genet*. 1995;4(1):93-8.
7. Khan AO, Becirovic E, Betz C, Neuhaus C, Altmuller J, Maria Riedmayr L, Motameny S, Nurnberg G, Nurnberg P, Bolz HJ. A deep intronic *CLRN1* (*USH3A*) founder mutation generates an aberrant exon and underlies severe Usher syndrome on the Arabian Peninsula. *Sci Rep*. 2017;7(1):1411.
8. Scotti MM, Swanson MS. RNA mis-splicing in disease. *Nat Rev Genet*. 2016;17(1):19-32.
9. Sterne-Weiler T, Sanford JR. Exon identity crisis: disease-causing mutations that disrupt the splicing code. *Genome Biol*. 2014;15(1):201.
10. Singh RK, Cooper TA. Pre-mRNA splicing in disease and therapeutics. *Trends Mol Med*. 2012;18(8):472-82.
11. Vaz-Drago R, Custodio N, Carmo-Fonseca M. Deep intronic mutations and human disease. *Hum Genet*. 2017;136(9):1093-111.
12. Sangermano R, Garanto A, Khan M, Runhart EH, Bauwens M, Bax NM, van den Born LI, Khan MI, Cornelis SS, Verheij J, Pott JR, Thiadens A, Klaver CCW, Puech B, Meunier I, Naessens S, Arno G, Fakin A, Carss KJ, Raymond FL, Webster AR, Dhaenens CM, Stohr H, Grassmann F, Weber BHF, Hoyng CB, De Baere E, Albert S, Collin RWJ, Cremers FPM. Deep-intronic *ABCA4* variants explain missing heritability in Stargardt disease and allow correction of splice defects by antisense oligonucleotides. *Genet Med*. 2019;21(8):1751-60.
13. Bax NM, Sangermano R, Roosing S, Thiadens AA, Hoefsloot LH, van den Born LI, Phan M, Klevering BJ, Westeneng-van Haften C, Braun TA, Zonneveld-Vrieling MN, de Wijs I, Mutlu M, Stone EM, den Hollander AI, Klaver CC, Hoyng CB, Cremers FP. Heterozygous deep-intronic variants and deletions in *ABCA4* in persons with retinal dystrophies and one exonic *ABCA4* variant. *Hum Mutat*. 2015;36(1):43-7.
14. Carss KJ, Arno G, Erwood M, Stephens J, Sanchis-Juan A, Hull S, Megy K, Grozeva D, Dewhurst E, Malka S, Plagnol V, Penkett C, Stirrups K, Rizzo R, Wright G, Josifova D, Bitner-Glindzicz M, Scott RH, Clement E, Allen L, Armstrong R, Brady AF, Carmichael J, Chitre M, Henderson RHH, Hurst J, MacLaren RE, Murphy E, Paterson J, Rosser E, Thompson DA, Wakeling E, Ouwehand WH, Michaelides M, Moore AT, Consortium NI-BRD, Webster AR, Raymond FL. Comprehensive Rare Variant Analysis via Whole-Genome Sequencing to Determine the Molecular Pathology of Inherited Retinal Disease. *Am J Hum Genet*. 2017;100(1):75-90.
15. Liquori A, Vache C, Baux D, Blanchet C, Hamel C, Malcolm S, Koenig M, Claustres M, Roux AF. Whole *USH2A* Gene Sequencing Identifies Several New Deep Intronic Mutations. *Hum Mutat*. 2016;37(2):184-93.

16. Mayer AK, Rohrschneider K, Strom TM, Glockle N, Kohl S, Wissinger B, Weisschuh N. Homozygosity mapping and whole-genome sequencing reveals a deep intronic PROM1 mutation causing cone-rod dystrophy by pseudoexon activation. *Eur J Hum Genet.* 2016;24(3):459-62.
17. Geng R, Geller SF, Hayashi T, Ray CA, Reh TA, Birmingham-McDonogh O, Jones SM, Wright CG, Melki S, Imanishi Y, Palczewski K, Alagramam KN, Flannery JG. Usher syndrome IIIA gene *clarin-1* is essential for hair cell function and associated neural activation. *Hum Mol Genet.* 2009;18(15):2748-60.
18. Becirovic E, Bohm S, Nguyen ON, Riedmayr LM, Koch MA, Schulze E, Kohl S, Borsch O, Santos-Ferreira T, Ader M, Michalakis S, Biel M. In Vivo Analysis of Disease-Associated Point Mutations Unveils Profound Differences in mRNA Splicing of Peripherin-2 in Rod and Cone Photoreceptors. *PLoS Genet.* 2016;12(1):e1005811.
19. Tan E, Ding XQ, Saadi A, Agarwal N, Naash MI, Al-Ubaidi MR. Expression of cone-photoreceptor-specific antigens in a cell line derived from retinal tumors in transgenic mice. *Invest Ophthalmol Vis Sci.* 2004;45(3):764-8.
20. Komor AC, Badran AH, Liu DR. CRISPR-Based Technologies for the Manipulation of Eukaryotic Genomes. *Cell.* 2017;169(3):559.
21. Dunn KC, Aotaki-Keen AE, Putkey FR, Hjelmeland LM. ARPE-19, a human retinal pigment epithelial cell line with differentiated properties. *Exp Eye Res.* 1996;62(2):155-69.
22. Ruan GX, Barry E, Yu D, Lukason M, Cheng SH, Scaria A. CRISPR/Cas9-Mediated Genome Editing as a Therapeutic Approach for Leber Congenital Amaurosis 10. *Mol Ther.* 2017;25(2):331-41.
23. Slijkerman RW, Vache C, Dona M, Garcia-Garcia G, Claustres M, Hetterschijt L, Peters TA, Hartel BP, Pennings RJ, Millan JM, Aller E, Garanto A, Collin RW, Kremer H, Roux AF, Van Wijk E. Antisense Oligonucleotide-based Splice Correction for USH2A-associated Retinal Degeneration Caused by a Frequent Deep-intronic Mutation. *Mol Ther Nucleic Acids.* 2016;5(10):e381.
24. Duijkers L, van den Born LI, Neidhardt J, Bax NM, Pierrache LHM, Klevering BJ, Collin RWJ, Garanto A. Antisense Oligonucleotide-Based Splicing Correction in Individuals with Leber Congenital Amaurosis due to Compound Heterozygosity for the c.2991+1655A>G Mutation in CEP290. *Int J Mol Sci.* 2018;19(3).
25. Garanto A, Duijkers L, Tomkiewicz TZ, Collin RWJ. Antisense Oligonucleotide Screening to Optimize the Rescue of the Splicing Defect Caused by the Recurrent Deep-Intronic ABCA4 Variant c.4539+2001G>A in Stargardt Disease. *Genes (Basel).* 2019;10(6).
26. Maeder ML, Stefanidakis M, Wilson CJ, Baral R, Barrera LA, Bounoutas GS, Bumcrot D, Chao H, Ciulla DM, DaSilva JA, Dass A, Dhanapal V, Fennell TJ, Friedland AE, Giannoukos G, Gloskowski SW, Glucksmann A, Gotta GM, Jayaram H, Haskett SJ, Hopkins B, Horng JE, Joshi S, Marco E, Mepani R, Reyon D, Ta T, Tabbaa DG, Samuelsson SJ, Shen S, Skor MN, Stetkiewicz P, Wang T, Yudkoff C, Myer VE, Albright CF, Jiang H. Development of a gene-editing approach to restore vision loss in Leber congenital amaurosis type 10. *Nat Med.* 2019;25(2):229-33.
27. Cideciyan AV, Jacobson SG, Drack AV, Ho AC, Charng J, Garafalo AV, Roman AJ, Sumaroka A, Han IC, Hochstedler MD, Pfeifer WL, Sohn EH, Taiel M, Schwartz MR, Biasutto P, Wit W, Cheetham ME, Adamson P, Rodman DM, Platenburg G, Tome MD, Balikova I, Nerinckx F, Zaeytijd J, Van Cauwenbergh C, Leroy BP, Russell SR. Effect of an intravitreal antisense oligonucleotide on vision in Leber congenital amaurosis due to a photoreceptor cilium defect. *Nat Med.* 2019;25(2):225-8.
28. Becirovic E, Bohm S, Nguyen ON, Riedmayr LM, Hammelmann V, Schon C, Butz ES, Wahl-Schott C, Biel M, Michalakis S. AAV Vectors for FRET-Based Analysis of Protein-Protein Interactions in Photoreceptor Outer Segments. *Front Neurosci.* 2016;10:356.
29. Bohm S, Riedmayr LM, Nguyen ONP, Giessl A, Liebscher T, Butz ES, Schon C, Michalakis S, Wahl-Schott C, Biel M, Becirovic E. Peripherin-2 and Rom-1 have opposing effects on rod outer segment targeting of retinitis pigmentosa-linked peripherin-2 mutants. *Sci Rep.* 2017;7(1):2321.

30. Trapani I, Colella P, Sommella A, Iodice C, Cesi G, de Simone S, Marrocco E, Rossi S, Giunti M, Palfi A, Farrar GJ, Polishchuk R, Auricchio A. Effective delivery of large genes to the retina by dual AAV vectors. *EMBO Mol Med*. 2014;6(2):194-211.
31. Amoasii L, Hildyard JCW, Li H, Sanchez-Ortiz E, Mireault A, Caballero D, Harron R, Stathopoulou TR, Massey C, Shelton JM, Bassel-Duby R, Piercy RJ, Olson EN. Gene editing restores dystrophin expression in a canine model of Duchenne muscular dystrophy. *Science*. 2018;362(6410):86-91.
32. Moretti A, Fonteyne L, Giesert F, Hoppmann P, Meier AB, Bozoglu T, Baehr A, Schneider CM, Sinnecker D, Klett K, Frohlich T, Rahman FA, Haufe T, Sun S, Jurisch V, Kessler B, Hinkel R, Dirschinger R, Martens E, Jilek C, Graf A, Krebs S, Santamaria G, Kurome M, Zakhartchenko V, Campbell B, Voelse K, Wolf A, Ziegler T, Reichert S, Lee S, Flenkenthaler F, Dorn T, Jeremias I, Blum H, Dendorfer A, Schnieke A, Krause S, Walter MC, Klymiuk N, Laugwitz KL, Wolf E, Wurst W, Kupatt C. Somatic gene editing ameliorates skeletal and cardiac muscle failure in pig and human models of Duchenne muscular dystrophy. *Nat Med*. 2020;26(2):207-14.
33. Oberbauer R. Not nonsense but antisense--applications of antisense oligonucleotides in different fields of medicine. *Wien Klin Wochenschr*. 1997;109(2):40-6.
34. Li B, Zeng C, Li W, Zhang X, Luo X, Zhao W, Zhang C, Dong Y. Synthetic Oligonucleotides Inhibit CRISPR-Cpf1-Mediated Genome Editing. *Cell Rep*. 2018;25(12):3262-72 e3.
35. Riedmayr LM, Böhm, S., Michalakis, S. and Becirovic, E. Construction and Cloning of Minigenes for in vivo Analysis of Potential Splice Mutations. *Bio-protocol* 2018;8(5):e2760.
36. Michalakis S, Muhlfriedel R, Tanimoto N, Krishnamoorthy V, Koch S, Fischer MD, Becirovic E, Bai L, Huber G, Beck SC, Fahl E, Buning H, Paquet-Durand F, Zong X, Gollisch T, Biel M, Seeliger MW. Restoration of cone vision in the CNGA3^{-/-} mouse model of congenital complete lack of cone photoreceptor function. *Mol Ther*. 2010;18(12):2057-63.
37. Swiech L, Heidenreich M, Banerjee A, Habib N, Li Y, Trombetta J, Sur M, Zhang F. In vivo interrogation of gene function in the mammalian brain using CRISPR-Cas9. *Nat Biotechnol*. 2015;33(1):102-6.
38. al-Ubaidi MR, Font RL, Quiambao AB, Keener MJ, Liou GI, Overbeek PA, Baehr W. Bilateral retinal and brain tumors in transgenic mice expressing simian virus 40 large T antigen under control of the human interphotoreceptor retinoid-binding protein promoter. *J Cell Biol*. 1992;119(6):1681-7.
39. Jat PS, Cepko CL, Mulligan RC, Sharp PA. Recombinant retroviruses encoding simian virus 40 large T antigen and polyomavirus large and middle T antigens. *Mol Cell Biol*. 1986;6(4):1204-17.
40. Xu J. Preparation, culture, and immortalization of mouse embryonic fibroblasts. *Curr Protoc Mol Biol*. 2005;Chapter 28:Unit 28 1.
41. Li H. Aligning sequence reads, clone sequences and assembly contigs with BWA-MEM. *arXiv*. 2013;arXiv:1303.3997.
42. DePristo MA, Banks E, Poplin R, Garimella KV, Maguire JR, Hartl C, Philippakis AA, del Angel G, Rivas MA, Hanna M, McKenna A, Fennell TJ, Kernysky AM, Sivachenko AY, Cibulskis K, Gabriel SB, Altshuler D, Daly MJ. A framework for variation discovery and genotyping using next-generation DNA sequencing data. *Nat Genet*. 2011;43(5):491-8.
43. Van der Auwera GA, Carneiro MO, Hartl C, Poplin R, Del Angel G, Levy-Moonshine A, Jordan T, Shakir K, Roazen D, Thibault J, Banks E, Garimella KV, Altshuler D, Gabriel S, DePristo MA. From FastQ data to high confidence variant calls: the Genome Analysis Toolkit best practices pipeline. *Curr Protoc Bioinformatics*. 2013;43:11 0 1- 0 33.
44. Picelli S, Bjorklund AK, Faridani OR, Sagasser S, Winberg G, Sandberg R. Smart-seq2 for sensitive full-length transcriptome profiling in single cells. *Nat Methods*. 2013;10(11):1096-8.
45. Dobin A, Davis CA, Schlesinger F, Drenkow J, Zaleski C, Jha S, Batut P, Chaisson M, Gingeras TR. STAR: ultrafast universal RNA-seq aligner. *Bioinformatics*. 2013;29(1):15-21.
46. Li B, Dewey CN. RSEM: accurate transcript quantification from RNA-Seq data with or without a reference genome. *BMC Bioinformatics*. 2011;12:323.

47. Dalkara D, Byrne LC, Klimczak RR, Visel M, Yin L, Merigan WH, Flannery JG, Schaffer DV. In vivo-directed evolution of a new adeno-associated virus for therapeutic outer retinal gene delivery from the vitreous. *Sci Transl Med.* 2013;5(189):189ra76.
48. Khabou H, Desrosiers M, Winckler C, Fouquet S, Auregan G, Bemelmans AP, Sahel JA, Dalkara D. Insight into the mechanisms of enhanced retinal transduction by the engineered AAV2 capsid variant -7m8. *Biotechnol Bioeng.* 2016;113(12):2712-24.
49. Petrs-Silva H, Dinculescu A, Li Q, Min SH, Chiodo V, Pang JJ, Zhong L, Zolotukhin S, Srivastava A, Lewin AS, Hauswirth WW. High-efficiency transduction of the mouse retina by tyrosine-mutant AAV serotype vectors. *Mol Ther.* 2009;17(3):463-71.
50. Koch S, Sothilingam V, Garcia Garrido M, Tanimoto N, Becirovic E, Koch F, Seide C, Beck SC, Seeliger MW, Biel M, Muhlriedel R, Michalakis S. Gene therapy restores vision and delays degeneration in the CNGB1(-/-) mouse model of retinitis pigmentosa. *Hum Mol Genet.* 2012;21(20):4486-96.

Supplementary information

Anna-Lena Panagiotopoulos², Nina Karguth^{1,2}, Marina Pavlou^{2,3}, Sybille Böhm^{1,2}, Gilles Gasparoni⁴, Jörn Walter⁴, Alexander Graf⁵, Helmut Blum⁵, Martin Biel^{1,2}, Lisa Maria Riedmayr^{1,2*}, and Elvir Becirovic^{1,2*}

¹Center for Integrated Protein Science Munich CIPSM

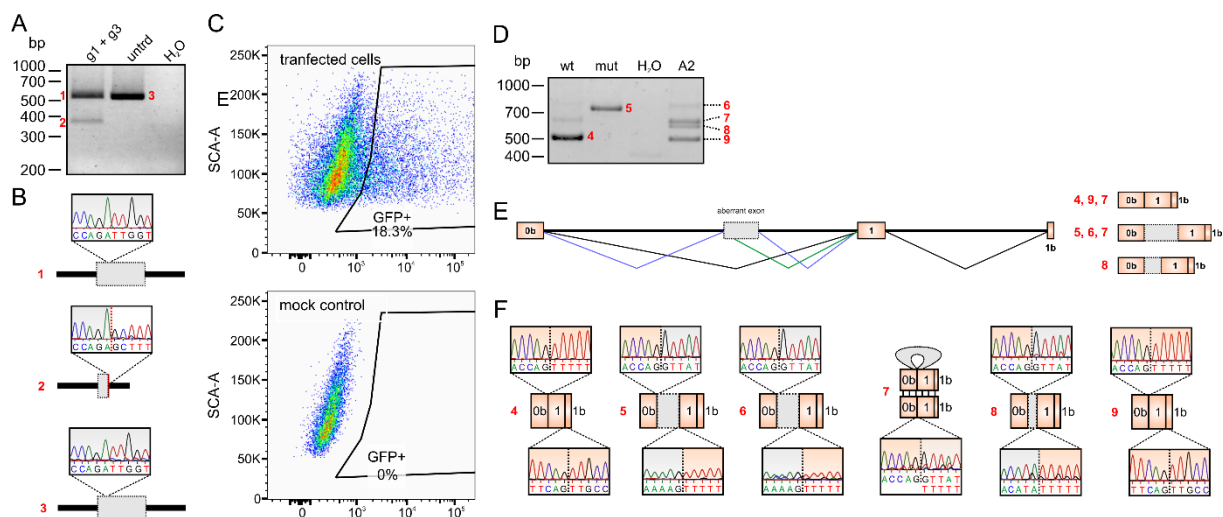
²Department of Pharmacy - Center for Drug Research, Ludwig-Maximilians-Universität München, Germany

³Department of Ophthalmology - Munich Eye Hospital
Ludwig-Maximilians-Universität München, Germany

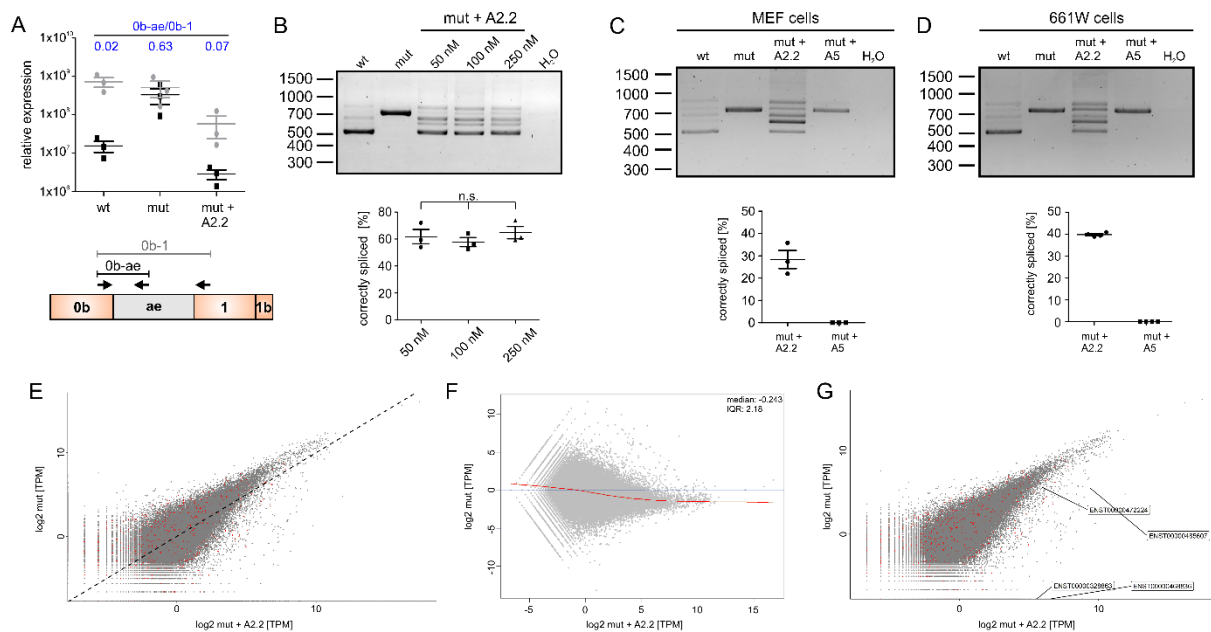
⁴Department of Genetics, Saarland University, Germany

⁵Gene Center Munich, Ludwig-Maximilians-Universität München, Germany

*corresponding author

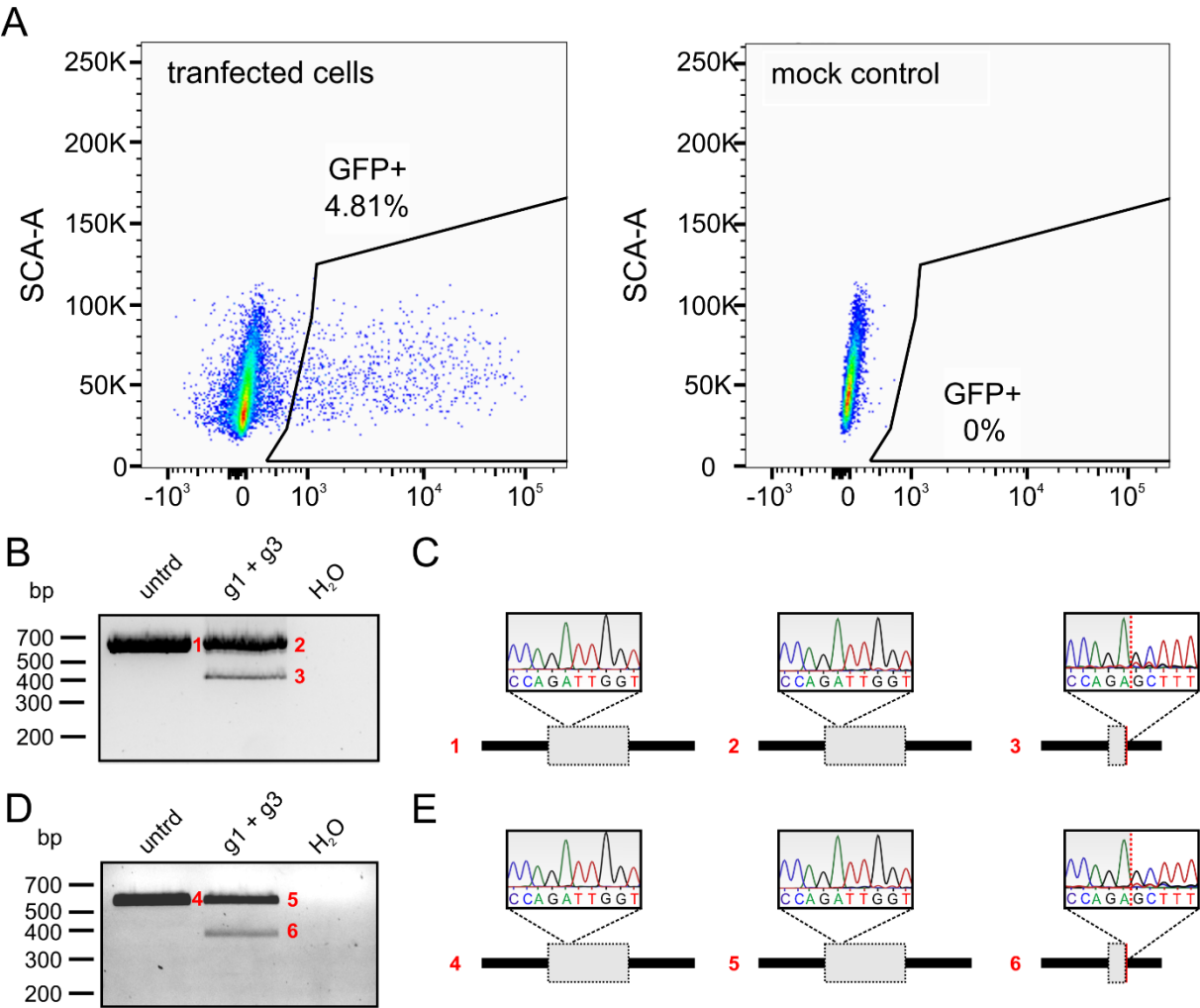


Suppl. Fig. 1 Sequencing of the edited *CLRN1* locus and the *CLRN1* transcript. A, PCR amplifying the genomic endogenous wild type *CLRN1* locus originating from HEK293 cells expressing the *SpCas9* with the g1 + g3 combination. untrd, untreated. B, Sequencing results of the bands depicted in A. The grey box represents the aberrant exon. The excision induced by the catalytic activity of the *SpCas9* is indicated with a dashed red line. C, Transiently transfected HEK293 cells sorted for nascent GFP fluorescence. Cells transfected with a *SpCas9* construct without a fluorophore were used as a mock control (lower panel). SCA, single channel analyzer. D, RT-PCR from HEK293 cells transiently expressing wild type (wt) or mutant (mut) *CLRN1* minigenes or the mutant minigene in combination with A2. E, Scheme depicting the single splicing events (highlighted in different colors) occurring between exon 0b and exon 1 of the *CLRN1* pre-mRNA as detected in D. F, Sequencing results of the different *CLRN1* transcript variants shown in D. Band number 7 represents a hybrid band consisting of correctly spliced transcript and mutated transcript which can be formed during the PCR cycling conditions.

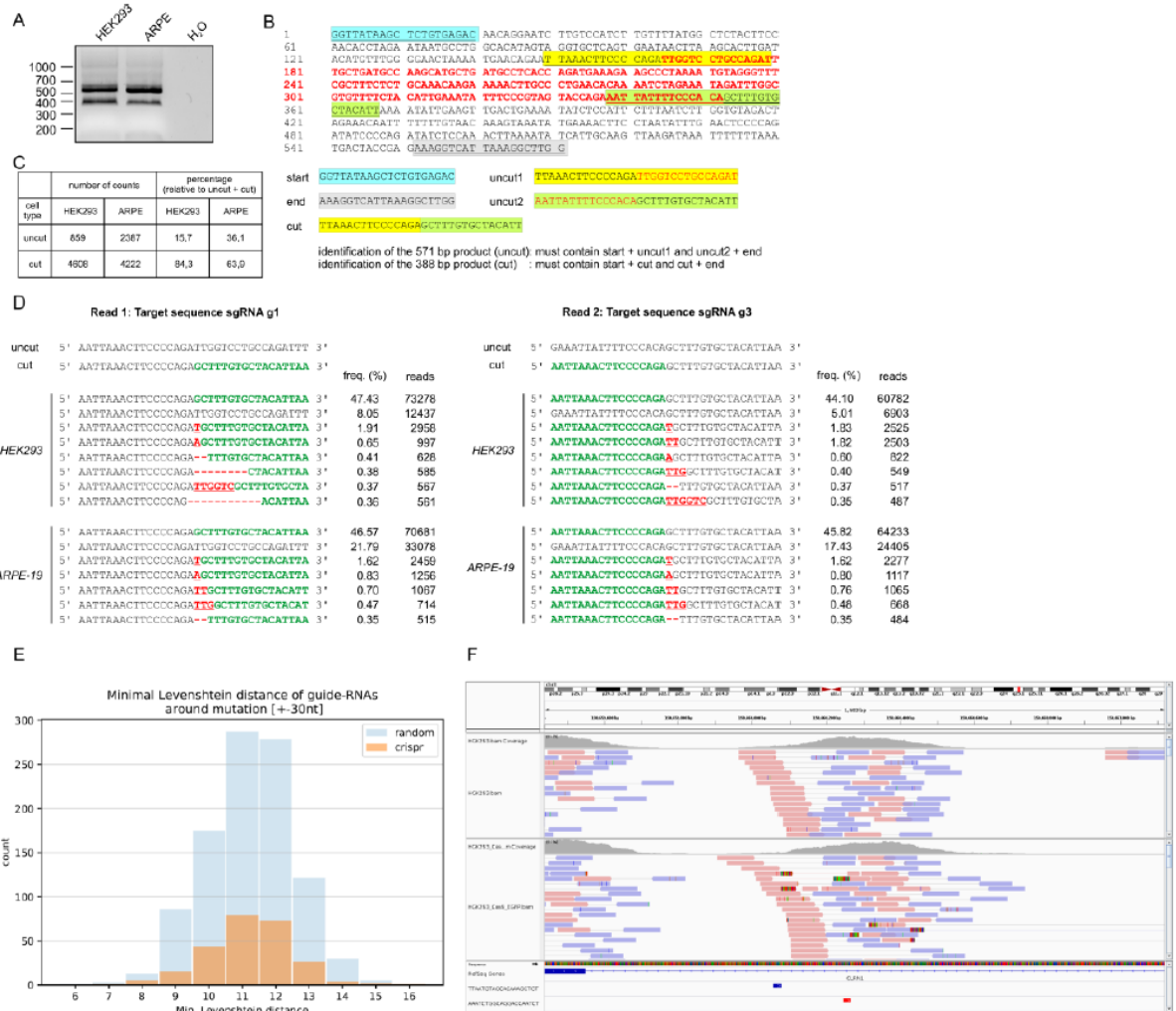


Suppl. Fig. 2 A, qRT-PCR from HEK293 cells transiently transfected with the single *CLRN1* minigenes in presence or absence of A2.2 as indicated. Each lane contains two data sets originating from the primer combinations amplifying the aberrantly spliced *CLRN1* (0b-ae) or both correctly and aberrantly spliced *CLRN1* (0b-1) as depicted in the lower panel. The 0b-ae/0b-1 ratio for the single combinations is shown above the corresponding relative expression values. B, Representative RT-PCR showing splicing correction efficiency in relation to different A2.2 concentrations. The corresponding quantification based on the densitometric PCR band analysis is shown below. Statistical analysis was done with one-way ANOVA followed by a Benferroni's post-hoc test. n.s., not significant. C-D, Representative RT-PCR from MEF (C) or 661W cells (D) including the densitometric quantification for the single transfections as indicated. Statistical analysis was conducted using the unpaired t-test. ***, $p \leq 0.001$. E-F, RNA-seq scatter plots from HEK293 cells transfected with the mutant *CLRN1* minigene in presence (x-axis) or absence (y-axis) of A2.2. Red dots in the scatter plots illustrate the potential off-target transcripts ($n = 1978$, details see Methods). Expression of the four annotated *CLRN1* transcripts as highlighted. TPM, transcripts per kilobase million. F, MA-plot:

The red line indicates the overall reduction of gene expression in the mut + A2.2 sample as compared to the dashed blue line.



Suppl. Fig. 3 FAC-sorting of ARPE-19 cells and sequencing of edited *CLRN1* locus in ARPE-19 and hRPE cells. A, Transiently transfected ARPE-19 cells sorted for nascent GFP fluorescence. Cells transfected with a *SpCas9*/sgRNA construct without a fluorophore were used as a mock control (right panel). SCA, single channel analyzer. B, PCR from genomic DNA isolated from transiently transfected and FAC-sorted APRE-19 cells. untd, untreated. C, Sequencing results of the bands depicted in B. The grey box represents the aberrant exon. The excision induced by catalytic activity of the *SpCas9* is indicated with a dashed red line. D, PCR from genomic DNA isolated from transduced hRPE cells one week post-infection. E, Sequencing results of the bands depicted in D.



Suppl. Fig. 4. Quantification and off-target effects of the gene editing using NGS. A, Co-purified PCR amplicons from sorted HEK293 and ARPE-19 cells used for targeted NGS. **B,** Sequence of the PCR amplicon and strategy for quantification. Red letters indicate the region which will be removed from the *CLRN1* locus upon *SpCas9* cleavage in presence of g1 + g3. Due to the sequencing length (up to 250 bp from both molecule ends), the uncut or cut sequence (571 bp vs. 388 bp) could not be identified as one single entity for quantification. The strategy for detecting these products is based on the characteristic sequences present in the cut or uncut products as highlighted by the different colors and as explained in the text below the sequence. **C,** Quantification of the reads for the single bands and cell types as indicated. **D,** List of most frequent *CLRN1* sequences identified using targeted NGS. The cut-off value was set to 0.35 %. The uncut and cut *CLRN1* sequences are listed on top for reference. Read 1 (left panel) and read 2 (right panel) covered the target sequence of sgRNA

g1 and g3, respectively. freq, frequency. E, Levenshtein distances of sgRNAs around identified variants. The histogram in orange shows the number of minimal Levenshtein distances from the alignments of the two sgRNAs (g1 and g3) to all variants specific to SpCas9 treated HEK293 cells within a sliding window 30 bp up- and downstream of the variant position. The blue histogram shows the minimal distances from 1,000 randomly chosen genomic positions. At least seven base modifications (exchange, deletion, insertion) would be required around the candidate regions of each variant to match one of the two sgRNAs. This indicates that these variants do not represent off-target effects. F, IGV browser plots of untreated and treated HEK293 cells in the *CLRN1* locus. Forward and reverse mapped reads were colored pink and blue, respectively. The targets of the two sgRNAs (g1 and g3) are highlighted as blue and red rectangles in the bottom.

Suppl. Table 1 Sequences of antisense oligonucleotides and masked splicing elements

AON	Sequence	Masking of
A1	5' GGACAAGAUUCCUGUUGUCUC 3'	SRSF1, SRSF2, SRSF5 & SRSF6 motifs
A2	5' UUCAUCUGGUGAGGCAUCAG 3'	SRSF1, SRSF5 & SRSF6 motifs
A3	5' CGAAACCCUACCUUUUAGGG 3'	SRSF1 motif & novel donor splice site
A4	5' UUUUAGGGCUUCUUUCAUCU 3'	Novel donor splice site
A5	5' UGCAGAGAAAGCGAAACCCU 3'	ISE motif group A (51)
A2.1	5' UUCAUCUGGUGAGGCAUC 3'	SRSF1, SRSF5 & SRSF6 motifs
A2.2	5' CUUUCAUCUGGUGAGGCAUCAGC 3'	SRSF1, SRSF5 & SRSF6 motifs
A2.3	5' CUGGUGAGGCAUCAGCAUGC 3'	SRSF1, SRSF5 & SRSF6 motifs

Suppl. Table 2 sgRNA targeting sequences. The corresponding PAM sequences are shown in italic.

sgRNA targeting sequences	
<i>CLRN1</i> g1	5' AAATCTGGCAGGACCAATCT <i>TGG</i> 3'
<i>CLRN1</i> g2	5' TGGTGAGGCATCAGCATGCT <i>TGG</i> 3'
<i>CLRN1</i> g3	5' TTAATGTAGCACAAAGCTGT <i>GGG</i> 3'
<i>CLRN1</i> g4	5' TCTACACCAAGATTAAGAA <i>TGG</i> 3'

Suppl. Table 3 Primers used in this study.

Primer name	Sequence 5' – 3'
<i>CLRN1</i> exon0b forward	TTGACCCCTTCATGGGACTC
<i>CLRN1</i> exon1b reverse	TTGAGCCTGGTGCCTGGTA
pcDNA3.1 forward	ACTATAGGGAGACCCAAGCTG
piggybac forward	CCATCCACGCTGTTTTGACC
<i>CLRN1</i> genomic intron forward	GGTTATAAGCTCTGTGAGACAAC
<i>CLRN1</i> genomic intron reverse	CCAAGCCTTTAATGACCTTTCTCG
qPCR <i>CLRN1</i> exon 1 forward	CATGGTCCCCTAGGGCTGTACC
qPCR <i>CLRN1</i> exon 1b reverse	GCCTGGTAGCTGGCAGCCAAA
qPCR <i>CLRN1</i> exon 0b-ae or 0b-1 forward	AAACTCCATGCAGGCCCTGC
qPCR <i>CLRN1</i> exon 0b-ae reverse	CAGGACCAATCTGGGGAAGTT
qPCR <i>CLRN1</i> exon 0b-1 reverse	GGCTGTCCCCACCATGGTTA
qPCR CLRN1 plasmid forward	TTGCCCTTTGGCTGCCAGC
qPCR CLRN1 plasmid reverse	GGTGGCGACCGGTAGATCTAT
CLRN1 NGS forward	TCTTTCCCTACACGACGCTCTTCCGATCTG GTTATAAGCTCTGTGAGACAAC
CLRN1 NGS reverse	GTGACTGGAGTTCAGACGTGTGCTCTTCC GATCTCCAAGCCTTTAATGACCTTTCTCG
<i>CLRN1</i> exon1b + SV40pA reverse	GCCATGGACCGGTCTTGAGCC

3 Discussion

I have tested two promising therapeutic approaches to pave the way for the more advanced pre-clinical trial to treat USH3A patients carrying the deep intronic c.254-649T>G *CLRN1* splicing mutation. In this context, I evaluated the potential of CRISPR-Cas9 and antisense-oligonucleotide-based gene editing, two technologies working at the DNA or pre-mRNA level, respectively [103]. Both approaches were tested in different human and murine cells lines, and yielded reasonable splice rescue efficiency. Moreover, AONs could rescue the mRNA splicing to a considerable extent in the mouse retina. Walmsley et al. used AONs for the treatment of the muscular phenotype in Cavalier King Charles Spaniels, carrying a naturally occurring mutation in the Duchenne muscular dystrophy (*DMD*) gene [104]. This missense mutation leads to a frameshift resulting in a truncated protein [104]. By the help of AON-based gene editing, they were able to restore the reading frame in myoblasts obtained from affected dogs. In another study, Amoasii et al. could restore the reading frame in another dog model for Duchenne muscular dystrophy (DMD), using the CRISPR-Cas9 technology [105]. Moreover, a recently published work showed a morphological and functional improvement in a pig model for DMD treated with Cas9 designed to cut out the exon harboring the mutation and resulted in a restoration of the reading frame [106]. AONs have been utilized in the past for the treatment of splicing mutations for LCA, Usher syndrome type II (USH2) or Stargardt disease [54], [107], [108]. These findings led to first clinical trials using AONs for patients carrying the most common deep-intronic c.2991+1655A>G mutation in *CEP290* gene [109], [110]. These findings outline the great potential of AON and CRISPR-Cas9-based technologies for future therapies. An advantage of AONs is their easy way of application as naked molecules and the high efficiency to be taken up by the different retinal cell types. Another important advantage of AONs is their relatively cost-friendly production in contrast to recombinant adeno-associated viruses (rAAVs), whose production is costly and time-consuming. However, AON administration must be applied continuously in intervals of a few months in contrast of CRISPR-Cas9 approach, where a single administration is sufficient. Such frequent administration enhances the risk of adverse effects and collateral damage for

the patients. Using the minimal cytomegalovirus (CMV) vector, Cas9 can be efficiently expressed in all retinal cell types [93]. However, also this technology has its limiting factors, e.g. the large size of the different Cas9 modules, which (depending on the Cas type and vector design) can violate the DNA packaging capacity of AAV vectors. This means that *SpCas9* and sgRNA cassette typically need to be delivered via two separate rAAVs (dual AAV vectors). Dual AAV vectors, however further increase the costs and time investment for the production. In addition, dual AAVs require high co-transduction efficiency in the target cells. Nevertheless, studies have shown that the application of two rAAVs resulted in high levels of co-transduction [93], [111]–[113]. Furthermore, due to its bacterial origin, *SpCas9* increases the risk of immune responses in the target cells or tissues. However, several strategies have been provided in previous studies designed to ensure a transient expression of Cas9 [93] [114]. Finally, both CRISPR-Cas9 gene editing and AONs can induce off-target effects at the genome or transcriptome level, respectively. Whole exome sequencing (WES) and RNA sequencing (RNAseq) could exclude off-targets under the conditions used herein. Likewise, a recent published study reported about no apparent off-targets for a CRISPR-Cas9 based approach for LCA treatment in the retina [93]. However, it cannot be excluded that some off-targets could be detectable in a more native setting. In this study, I also show that there are no synergistic effects when combining AONs and CRISPR-Cas9 in a single approach. One plausible explanation could be that AONs bind to the target sequence at the genome and prevent the Cas9 complex from binding and/or cutting the DNA. Nevertheless, further experiments are required to evaluate this hypothesis, which could lead to the development of novel specific *SpCas9* inhibitors. Taken together, I show that the CRISPR-Cas9 as well as the AON approach provide a significant splice rescue for the deep intronic c.254-649T>G *CLRN1* splicing mutation with no apparent off-target effects. These promising results require further preclinical development that might result in first clinical trials of USH3A patients. The results shown here can be transferred to veterinary medicine and thus become important for the treatment of exonic or intronic splicing mutations like PRAs, CRDs or CSNB. Even though both approaches

bear some disadvantages and risks. The absence of alternatives to treat genetic disorders shifts the risk-benefit balance in favour of utilizing such gene editing technologies.

4 References

- [1] M. Hoon, H. Okawa, L. Della Santina, and R. O. L. Wong, "Functional architecture of the retina: Development and disease," *Prog. Retin. Eye Res.*, vol. 42, pp. 44–84, 2014.
- [2] P. Mathur and J. Yang, "Usher syndrome: Hearing loss, retinal degeneration and associated abnormalities," *Biochim. Biophys. Acta - Mol. Basis Dis.*, vol. 1852, no. 3, pp. 406–420, 2015.
- [3] Purves D, Augustine GJ, Fitzpatrick D, "The Retina," in *Neuroscience. 2nd edition*, Hindawi, 2001.
- [4] H. Kolb, N. Ralph, and F. Eduardo, *Webvision: The Organization of the Retina and Visual System*. 1995.
- [5] D. T. Hartong, E. L. Berson, and T. P. Dryja, "Retinitis pigmentosa Prevalence and inheritance patterns," *Lancet*, vol. 368, pp. 1795–1809, 2006.
- [6] M. U. Ali, M. S. U. Rahman, J. Cao, and P. X. Yuan, "Genetic characterization and disease mechanism of retinitis pigmentosa; current scenario," *3 Biotech*, vol. 7, no. 4, pp. 1–20, 2017.
- [7] S. Broadgate, J. Yu, S. M. Downes, and S. Halford, "Unravelling the genetics of inherited retinal dystrophies: Past, present and future," *Prog. Retin. Eye Res.*, vol. 59, pp. 53–96, 2017.
- [8] C. G. Maubaret *et al.*, "Autosomal dominant retinitis pigmentosa with intrafamilial variability and incomplete penetrance in two families carrying mutations in prpf8," *Investig. Ophthalmol. Vis. Sci.*, vol. 52, no. 13, pp. 9304–9309, 2011.
- [9] P. A. Winkler *et al.*, "A large animal model for CNGB1 autosomal recessive retinitis pigmentosa," *PLoS One*, vol. 8, no. 8, 2013.
- [10] V. Marigo, "Programmed cell death in retinal degeneration: Targeting apoptosis in photoreceptors as potential therapy for retinal degeneration," *Cell Cycle*, vol. 6, no. 6, pp. 652–655, 2007.
- [11] L. Pakarinen, K. Tuppurainen, P. Laippala, M. Mäntyjärvi, and H. Puhakka, "The

- ophthalmological course of Usher syndrome type III," *Int. Ophthalmol.*, vol. 19, no. 5, pp. 307–311, Sep. 1995.
- [12] P. J. M. Clements, D. R. Sargan, D. J. Gould, and S. M. Petersen-Jones, "Recent advances in understanding the spectrum of canine generalised progressive retinal atrophy," *J. Small Anim. Pract.*, vol. 37, no. 4, pp. 155–162, 1996.
- [13] Mellersh CS., "The genetics of eye disorders in the dog," *Canine Genet Epidemiol.*, vol. 1, no. 3, pp. 1–14, 2014.
- [14] G. M. Acland *et al.*, "Gene therapy restores vision in a canine model of childhood blindness," *Nat. Genet.*, vol. 28, no. 1, pp. 92–95, 2001.
- [15] A. Simon, U. Hellman, C. Wernstedt, and U. Eriksson, "The retinal pigment epithelial-specific 11-cis retinol dehydrogenase belongs to the family of short chain alcohol dehydrogenases," *J. Biol. Chem.*, vol. 270, no. 3, pp. 1107–1112, 1995.
- [16] J. xing Ma, L. Xu, D. K. Othersen, T. M. Redmond, and R. K. Crouch, "Cloning and localization of RPE65 mRNA in salamander cone photoreceptor cells," *Biochim. Biophys. Acta - Gene Struct. Expr.*, vol. 1443, no. 1–2, pp. 255–261, 1998.
- [17] T. M. Redmond *et al.*, "Rpe65 is necessary for production of 11-cis-vitamin A in the retinal visual cycle," *Nat. Genet.*, vol. 20, no. 4, pp. 344–351, 1998.
- [18] J. P. Van Hooser *et al.*, "Rapid restoration of visual pigment and function with oral retinoid in a mouse model of childhood blindness," *Proc. Natl. Acad. Sci. U. S. A.*, vol. 97, no. 15, pp. 8623–8628, 2000.
- [19] *Stellungnahme der Deutschen Ophthalmologischen Gesellschaft , der Retinologischen Gesellschaft und des Berufsverbandes der Augenärzte Deutschlands zur therapeutischen Anwendung von voretigene neparvovec-rzyl (Luxturna TM) in der Augenheilkunde.* 2019.
- [20] Hameed A., Abid A., Aziz A., Ismail M., Mehdi S.Q., and Khaliq S., "Evidence of RPGRIP1 gene mutations associated with recessive cone-rod dystrophy," *J Med Genet*, vol. 40, no. 8, pp. 616–619, 2003.
- [21] T. P. Dryja *et al.*, "Null RPGRIP1 alleles in patients with Leber congenital amaurosis,"

- Am. J. Hum. Genet.*, vol. 68, no. 5, pp. 1295–1298, 2001.
- [22] J. C. Booij *et al.*, “Identification of mutations in the AIPL1, CRB1, GUCY2D, RPE65, and RPGRIP1 genes in patients with juvenile retinitis pigmentosa.” *J. Med. Genet.*, vol. 42, no. 11, pp. 1–8, 2005.
- [23] F. M. Mowat *et al.*, “Topographical characterization of cone photoreceptors and the area centralis of the canine retina,” *Mol. Vis.*, vol. 14, no. December, pp. 2518–2527, 2008.
- [24] R. R. Bellone *et al.*, “Differential gene expression of TRPM1, the potential cause of congenital stationary night blindness and coat spotting patterns (LP) in the appaloosa horse (*Equus caballus*),” *Genetics*, vol. 179, no. 4, pp. 1861–1870, 2008.
- [25] I. Audo *et al.*, “TRPM1 Is Mutated in Patients with Autosomal-Recessive Complete Congenital Stationary Night Blindness,” *Am. J. Hum. Genet.*, vol. 85, no. 5, pp. 720–729, 2009.
- [26] C. Nunnery, J. P. Pickett, and K. L. Zimmerman, “Congenital stationary night blindness in a Thoroughbred and a Paso Fino,” *Vet. Ophthalmol.*, vol. 8, no. 6, pp. 415–419, 2005.
- [27] K. Narfström, K. Holland Deckman, and M. Menotti-Raymond, “The Domestic Cat as a Large Animal Model for Characterization of Disease and Therapeutic Intervention in Hereditary Retinal Blindness,” *J. Ophthalmol.*, vol. 2011, no. May 2014, pp. 1–8, 2011.
- [28] Narfström, “Hereditary and congenital ocular disease in the cat,” *J. Feline Med. Surg.*, vol. 1, no. 3, pp. 135–141, 1999.
- [29] H. C. Rah, D. J. Maggs, T. N. Blankenship, K. Narfstrom, and L. A. Lyons, “Early-onset, autosomal recessive, progressive retinal atrophy in Persian cats,” *Investig. Ophthalmol. Vis. Sci.*, vol. 46, no. 5, pp. 1742–1747, 2005.
- [30] R. Ofri *et al.*, “Characterization of an early-onset, autosomal recessive, progressive retinal degeneration in bengal cats,” *Investig. Ophthalmol. Vis. Sci.*, vol. 56, no. 9, pp. 5299–5308, 2015.
- [31] M. Menotti-Raymond, K. H. Deckman, V. David, J. Myrkalo, S. J. O’Brien, and K. Narfström, “Mutation discovered in a feline model of human congenital retinal blinding disease,” *Investig. Ophthalmol. Vis. Sci.*, vol. 51, no. 6, pp. 2852–2859, 2010.

- [32] S. Chen *et al.*, "Crx, a novel Otx-like paired-homeodomain protein, binds to and transactivates photoreceptor cell-specific genes," *Neuron*, vol. 19, no. 5, pp. 1017–1030, 1997.
- [33] R. Curtis, K. C. Barnett, and A. Leon, "An early-onset retinal dystrophy with dominant inheritance in the Abyssinian cat. Clinical and pathological findings," *Investig. Ophthalmol. Vis. Sci.*, vol. 28, no. 1, pp. 131–139, 1987.
- [34] S. Narfström, K. & Nilsson, "Progressive retinal atrophy in the Abyssinian cat: Electron microscopy," *Investig. Ophthalmol. Vis. Sci.*, no. 12, pp. 1569–1576, 1986.
- [35] K. Narfström, "Progressive retinal atrophy in the Abyssinian cat," *Investig. Ophthalmol. Sci.*, vol. 26, no. 2, pp. 193–200, 1985.
- [36] S. G. Jacobson, C. M. Kemp, K. Narfström, and S. E. G. Nilsson, "Rhodopsin levels and rod-mediated function in abyssinian cats with hereditary retinal degeneration," *Exp. Eye Res.*, vol. 49, no. 5, pp. 843–852, 1989.
- [37] S. L. Ness, "Genetic homogeneity and phenotypic variability among Ashkenazi Jews with Usher syndrome type III," *J. Med. Genet.*, vol. 40, no. 10, pp. 767–772, 2003.
- [38] W. J. Kimberling *et al.*, "Frequency of Usher syndrome in two pediatric populations: Implications for genetic screening of deaf and hard of hearing children," *Genet. Med.*, vol. 12, no. 8, pp. 512–516, 2010.
- [39] H. Västinsalo *et al.*, "Alternative splice variants of the USH3A gene Clarin 1 (CLRN1)," *Eur. J. Hum. Genet.*, vol. 19, no. 1, pp. 30–35, Jan. 2011.
- [40] D. Well *et al.*, "Defective myosin VIIA gene responsible for Usher syndrome type IB," *Nature*, vol. 374, no. 6517, pp. 60–61, 1995.
- [41] C. Petit *et al.*, "A defect in harmonin, a PDZ domain-containing protein expressed in the inner ear sensory hair cells, underlies Usher syndrome type 1C," *Nat. Genet.*, vol. 26, no. 1, pp. 51–55, 2000.
- [42] A. Gal *et al.*, "Mutation of CDH23, encoding a new member of the cadherin gene family, causes Usher syndrome type 1D.," *Nat. Genet.*, vol. 27, no. 1, pp. 108–112, 2001.
- [43] Z. M. Ahmed *et al.*, "Mutations of the Protocadherin Gene PCDH15 Cause Usher

- Syndrome Type 1F,” *Am. J. Hum. Genet.*, vol. 69, no. 1, pp. 25–34, 2001.
- [44] D. Weil *et al.*, “Usher syndrome type I G (USH1G) is caused by mutations in the gene encoding SANS, a protein that associates with the USH1C protein, harmonin,” *Hum. Mol. Genet.*, vol. 12, no. 5, pp. 463–471, 2003.
- [45] S. Riazuddin *et al.*, “Alterations of the CIB2 calcium-and integrin-binding protein cause Usher syndrome type 1J and nonsyndromic deafness DFNB48,” *Nat. Genet.*, vol. 44, no. 11, pp. 1265–1271, 2012.
- [46] J. D. Eudy *et al.*, “Mutation of a gene encoding a protein with extracellular matrix motifs in Usher syndrome type IIa,” *Science (80-.)*, vol. 280, no. 5370, pp. 1753–1757, 1998.
- [47] M. D. Weston, M. W. J. Luijendijk, K. D. Humphrey, C. Möller, and W. J. Kimberling, “Mutations in the VLGR1 Gene Implicate G-Protein Signaling in the Pathogenesis of Usher Syndrome Type II,” *Am. J. Hum. Genet.*, vol. 74, no. 2, pp. 357–366, 2004.
- [48] I. Ebermann *et al.*, “A novel gene for Usher syndrome type 2: Mutations in the long isoform of whirlin are associated with retinitis pigmentosa and sensorineural hearing loss,” *Hum. Genet.*, vol. 121, no. 2, pp. 203–211, 2007.
- [49] E. G. Puffenberger *et al.*, “Genetic mapping and exome sequencing identify variants associated with five novel diseases,” *PLoS One*, vol. 7, no. 1, 2012.
- [50] A. Adato *et al.*, “USH3A transcripts encode clarin-1, a four-transmembrane-domain protein with a possible role in sensory synapses,” *Eur. J. Hum. Genet.*, vol. 10, no. 6, pp. 339–350, 2002.
- [51] T. Joensuu *et al.*, “Mutations in a Novel Gene with Transmembrane Domains Underlie Usher Syndrome Type 3,” *Am. J. Hum. Genet.*, vol. 69, no. 4, pp. 673–684, 2001.
- [52] K. H. Pakarinen L., Karjalainen S., Simola K., Laippala P., “Usher’s syndrome type 3 in Finland.” pp. 613–617, 1995.
- [53] M. Zallocchi *et al.*, “Localization and expression of clarin-1, the Clrn1 gene product, in auditory hair cells and photoreceptors,” *Hear. Res.*, vol. 255, no. 1–2, pp. 109–120, Sep. 2009.
- [54] R. W. Slijkerman *et al.*, “Antisense Oligonucleotide-based Splice Correction for USH2A-

- associated Retinal Degeneration Caused by a Frequent Deep-intronic Mutation,” *Mol. Ther. - Nucleic Acids*, vol. 5, no. November, p. e381, 2016.
- [55] I. Sahly *et al.*, “Localization of usher 1 proteins to the photoreceptor calyceal processes, which are absent from mice,” *J. Cell Biol.*, vol. 199, no. 2, pp. 381–399, 2012.
- [56] S. F. Geller *et al.*, “CLRN1 is nonessential in the mouse retina but is required for cochlear hair cell development,” *PLoS Genet.*, vol. 5, no. 8, pp. 17–19, 2009.
- [57] M. C. Wahl, C. L. Will, and R. Lührmann, “The Spliceosome: Design Principles of a Dynamic RNP Machine,” *Cell*, vol. 136, no. 4, pp. 701–718, 2009.
- [58] L. R. Will CL, “Spliceosome structure and function.,” *Cold Spring Harb. Perspect. Biol.*, vol. 3, no. 7, p. a003707, 2011.
- [59] M. M. Scotti and Swanson M.S., “RNA mis-splicing in disease.,” *Nat Rev Genet.*, vol. 17, no. 1, pp. 19–32, 2016.
- [60] R. K. Singh and T. A. Cooper, “Pre-mRNA splicing in disease and therapeutics Splicing and regulation of gene expression,” vol. 18, no. 8, pp. 472–482, 2013.
- [61] T. Sterne-Weiler and J. R. Sanford, “Exon identity crisis: Disease-causing mutations that disrupt the splicing code,” *Genome Biol.*, vol. 15, no. 1, p. 201, 2014.
- [62] K. L. Fox-Walsh and K. J. Hertel, “Splice-site pairing is an intrinsically high fidelity process,” *Proc. Natl. Acad. Sci. U. S. A.*, vol. 106, no. 6, pp. 1766–1771, 2009.
- [63] R. Vaz-Drago, N. Custódio, and M. Carmo-Fonseca, “Deep intronic mutations and human disease,” *Hum. Genet.*, vol. 136, no. 9, pp. 1093–1111, 2017.
- [64] R. Sangermano *et al.*, “Deep-intronic ABCA4 variants explain missing heritability in Stargardt disease and allow correction of splice defects by antisense oligonucleotides,” *Genet. Med.*, vol. 21, no. 8, pp. 1751–1760, 2019.
- [65] A. O. Khan *et al.*, “A deep intronic CLRN1 (USH3A) founder mutation generates an aberrant exon and underlies severe Usher syndrome on the Arabian Peninsula,” *Sci. Rep.*, vol. 7, no. 1, pp. 1–10, 2017.
- [66] N. M. Bax *et al.*, “Heterozygous deep-intronic variants and deletions in ABCA4 in persons with retinal dystrophies and one exonic ABCA4 variant,” *Hum. Mutat.*, vol. 36,

- no. 1, pp. 43–47, 2015.
- [67] K. Carss *et al.*, “Comprehensive Rare Variant Analysis via Whole-Genome Sequencing to Determine the Molecular Pathology of Inherited Retinal Disease,” *Am. J. Hum. Genet.*, vol. 100, no. 1, pp. 75–90, 2017.
- [68] A. K. Mayer *et al.*, “Homozygosity mapping and whole-genome sequencing reveals a deep intronic PROM1 mutation causing cone-rod dystrophy by pseudoexon activation,” *Eur. J. Hum. Genet.*, vol. 24, no. 3, pp. 459–462, 2016.
- [69] G. Tian *et al.*, “Clarin-1, encoded by the usher syndrome III causative gene, forms a membranous microdomain: Possible role of clarin-1 in organizing the actin cytoskeleton,” *J. Biol. Chem.*, vol. 284, no. 28, pp. 18980–18993, 2009.
- [70] O. Ogun and M. Zallocchi, “Clarin-1 acts as a modulator of mechanotransduction activity and presynaptic ribbon assembly,” *J. Cell Biol.*, vol. 207, no. 3, pp. 375–391, 2014.
- [71] R. R. Fields *et al.*, “Usher syndrome type III: Revised genomic structure of the USH3 gene and identification of novel mutations,” *Am. J. Hum. Genet.*, vol. 71, no. 3, pp. 607–617, 2002.
- [72] E. Aller *et al.*, “Mutation screening of USH3 gene (clarin-1) in Spanish patients with Usher syndrome: Low prevalence and phenotypic variability,” *Clin. Genet.*, vol. 66, no. 6, pp. 525–529, 2004.
- [73] J. Isosomppi, H. Västinsalo, S. F. Geller, E. Heon, J. G. Flannery, and E. M. Sankila, “Disease-causing mutations in the CLRN1 gene alter normal CLRN1 protein trafficking to the plasma membrane,” *Mol. Vis.*, vol. 15, no. April, pp. 1806–1818, 2009.
- [74] S. Dad *et al.*, “Usher syndrome in Denmark: Mutation spectrum and some clinical observations,” *Mol. Genet. Genomic Med.*, vol. 4, no. 5, pp. 527–539, 2016.
- [75] R. Geng *et al.*, “Usher syndrome IIIA gene clarin-1 is essential for hair cell function and associated neural activation,” *Hum. Mol. Genet.*, vol. 18, no. 15, pp. 2748–2760, 2009.
- [76] J. A. Doudna and E. Charpentier, “The new frontier of genome engineering with CRISPR-Cas9,” *Science (80-.)*, vol. 346, no. 6213, 2014.
- [77] T. Gaj, C. A. Gersbach, and C. F. Barbas, “ZFN, TALEN, and CRISPR/Cas-based

- methods for genome engineering,” *Trends Biotechnol.*, vol. 31, no. 7, pp. 397–405, 2013.
- [78] O. Alkhnabashi, T. Meier, A. Mitrofanov, R. Backofen, and B. Voß, “CRISPR-Cas Bioinformatics,” *Methods*, no. July, 2019.
- [79] A. Bolotin, B. Quinquis, A. Sorokin, and S. Dusko Ehrlich, “Clustered regularly interspaced short palindrome repeats (CRISPRs) have spacers of extrachromosomal origin,” *Microbiology*, vol. 151, no. 8, pp. 2551–2561, 2005.
- [80] F. J. M. Mojica, C. Díez-Villaseñor, J. García-Martínez, and E. Soria, “Intervening sequences of regularly spaced prokaryotic repeats derive from foreign genetic elements,” *J. Mol. Evol.*, vol. 60, no. 2, pp. 174–182, 2005.
- [81] K. S. Makarova, N. V. Grishin, S. A. Shabalina, Y. I. Wolf, and E. V. Koonin, “A putative RNA-interference-based immune system in prokaryotes: Computational analysis of the predicted enzymatic machinery, functional analogies with eukaryotic RNAi, and hypothetical mechanisms of action,” *Biol. Direct*, vol. 1, pp. 1–26, 2006.
- [82] K. S. Makarova, L. Aravind, N. V. Grishin, I. B. Rogozin, and E. V. Koonin, “A DNA repair system specific for thermophilic Archaea and bacteria predicted by genomic context analysis,” *Nucleic Acids Res.*, vol. 30, no. 2, pp. 482–496, Jan. 2002.
- [83] C. P. Guy, A. I. Majerník, J. P. J. Chong, and E. L. Bolt, “A novel nuclease-ATPase (Nar71) from archaea is part of a proposed thermophilic DNA repair system,” *Nucleic Acids Res.*, vol. 32, no. 21, pp. 6176–6186, 2004.
- [84] K. S. Makarova *et al.*, “Evolution and classification of the CRISPR-Cas systems,” *Nat. Rev. Microbiol.*, vol. 9, no. 6, pp. 467–477, 2011.
- [85] K. S. Makarova, L. Aravind, Y. I. Wolf, and E. V. Koonin, “Unification of Cas protein families and a simple scenario for the origin and evolution of CRISPR-Cas systems,” *Biol. Direct*, vol. 6, no. 1, p. 38, 2011.
- [86] V. Ahmadzadeh, S. Farajnia, R. Baghban, L. Rahbarnia, and H. Zarredar, “CRISPR-Cas system: Toward a more efficient technology for genome editing and beyond,” *J. Cell. Biochem.*, no. February, 2019.

- [87] E. R. Westra *et al.*, “Type I-E CRISPR-Cas Systems Discriminate Target from Non-Target DNA through Base Pairing-Independent PAM Recognition,” *PLoS Genet.*, vol. 9, no. 9, 2013.
- [88] L. A. Marraffini and E. J. Sontheimer, “Self versus non-self discrimination during CRISPR RNA-directed immunity,” *Nature*, vol. 463, no. 7280, pp. 568–571, 2010.
- [89] M. D. Szczelkun *et al.*, “Direct observation of R-loop formation by single RNA-guided Cas9 and Cascade effector complexes,” *Proc. Natl. Acad. Sci.*, vol. 111, no. 27, pp. 9798–9803, 2014.
- [90] S. H. Sternberg *et al.*, “DNA interrogation by the CRISPR RNA-guided endonucleas,” *Nature*, vol. 507, no. 7490, pp. 62–67, 2014.
- [91] Martin Jinek, Krzysztof Chylinski, Ines Fonfara, Michael Hauer, Jennifer A. Doudna, and Emmanuelle Charpentier, “A Programmable Dual-RNA–Guided DNA Endonuclease in Adaptive Bacterial Immunity,” *Science (80-.)*, vol. 337, no. 6096, pp. 816–821, 2012.
- [92] G. Gasiunas, R. Barrangou, P. Horvath, and V. Siksnys, “Cas9-crRNA ribonucleoprotein complex mediates specific DNA cleavage for adaptive immunity in bacteria,” *Proc. Natl. Acad. Sci.*, vol. 109, no. 39, pp. E2579–E2586, 2012.
- [93] G. X. Ruan, E. Barry, D. Yu, M. Lukason, S. H. Cheng, and A. Scaria, “CRISPR/Cas9-Mediated Genome Editing as a Therapeutic Approach for Leber Congenital Amaurosis 10,” *Mol. Ther.*, vol. 25, no. 2, pp. 331–341, 2017.
- [94] D. R. Scoles, E. V. Minikel, and S. M. Pulst, “Antisense oligonucleotides: A primer,” *Neurol. Genet.*, vol. 5, no. 2, 2019.
- [95] C. F. Bennett and E. E. Swayze, “RNA Targeting Therapeutics: Molecular Mechanisms of Antisense Oligonucleotides as a Therapeutic Platform,” *Annu. Rev. Pharmacol. Toxicol.*, vol. 50, no. 1, pp. 259–293, 2010.
- [96] P. R. Sara Karaki, Clément Paris, “Antisense Oligonucleotides, A Novel Developing Targeting Therapy,” *Intech*, p. 13, 2019.
- [97] C. F. Bennett, B. F. Baker, N. Pham, E. Swayze, and R. S. Geary, “Pharmacology of Antisense Drugs,” *Annu. Rev. Pharmacol. Toxicol.*, vol. 57, no. 1, pp. 81–105, 2017.

- [98] R. S. Geary, D. Norris, R. Yu, and C. F. Bennett, "Pharmacokinetics, biodistribution and cell uptake of antisense oligonucleotides," *Adv. Drug Deliv. Rev.*, vol. 87, pp. 46–51, 2015.
- [99] R. L. Juliano, "The delivery of therapeutic oligonucleotides," *Nucleic Acids Res.*, vol. 44, no. 14, pp. 6518–6548, 2016.
- [100] Eckstein F1., "Phosphorothioates, essential components of therapeutic oligonucleotides.," *Nucleic Acid Ther.*, vol. 24, no. 6, pp. 374–387, 2014.
- [101] A. Garanto *et al.*, "In vitro and in vivo rescue of aberrant splicing in CEP290 -associated LCA by antisense oligonucleotide delivery," *Hum. Mol. Genet.*, vol. 25, no. 12, pp. 2552–2563, 2016.
- [102] S. P. Henry *et al.*, "Activation of the alternative pathway of complement by a phosphorothioate oligonucleotide: potential mechanism of action.," *J. Pharmacol. Exp. Ther.*, vol. 281, no. 2, pp. 810–816, 1997.
- [103] J. Kuhn *et al.*, "Supramolecular Assembly of Aminoethylene-Lipopeptide PMO Conjugates into RNA Splice-Switching Nanomicelles," *Adv. Funct. Mater.*, vol. 1906432, p. 1906432, 2019.
- [104] G. L. Walmsley *et al.*, "A duchenne muscular dystrophy gene hot spot mutation in dystrophin-deficient Cavalier King Charles Spaniels is amenable to exon 51 skipping," *PLoS One*, vol. 5, no. 1, 2010.
- [105] L. Amoasii *et al.*, "Gene editing restores dystrophin expression in a canine model of duchenne muscular dystrophy," *Science (80-.)*, vol. 362, no. 6410, pp. 86–91, 2018.
- [106] A. Moretti *et al.*, "Somatic gene editing ameliorates skeletal and cardiac muscle failure in pig and human models of Duchenne muscular dystrophy," *Nat. Med.*, 2020.
- [107] L. Duijkers *et al.*, "Antisense oligonucleotide-based splicing correction in individuals with leber congenital amaurosis due to compound heterozygosity for the c.2991+1655A>G mutation in CEP290," *Int. J. Mol. Sci.*, vol. 19, no. 3, pp. 1–12, 2018.
- [108] A. Garanto, L. Duijkers, T. Z. Tomkiewicz, and R. W. J. Collin, "Antisense Oligonucleotide Screening to Optimize the Rescue of the Splicing Defect Caused by the

- Recurrent Deep-Intronic ABCA4 Variant c.4539+2001G>A in Stargardt Disease,” *Genes (Basel)*, vol. 10, no. 6, p. 452, 2019.
- [109] A. V. Cideciyan *et al.*, “Effect of an intravitreal antisense oligonucleotide on vision in Leber congenital amaurosis due to a photoreceptor cilium defect,” *Nat. Med.*, vol. 25, no. 2, pp. 225–228, 2019.
- [110] M. L. Maeder *et al.*, “Development of a gene-editing approach to restore vision loss in Leber congenital amaurosis type 10,” *Nat. Med.*, vol. 25, no. 2, pp. 229–233, 2019.
- [111] E. Becirovic *et al.*, “AAV vectors for FRET-based analysis of protein-protein interactions in photoreceptor outer segments,” *Front. Neurosci.*, vol. 10, pp. 1–13, 2016.
- [112] E. Becirovic *et al.*, “In Vivo Analysis of Disease-Associated Point Mutations Unveils Profound Differences in mRNA Splicing of Peripherin-2 in Rod and Cone Photoreceptors,” *PLoS Genet.*, vol. 12, no. 1, pp. 1–22, 2016.
- [113] S. Böhm *et al.*, “Peripherin-2 and Rom-1 have opposing effects on rod outer segment targeting of retinitis pigmentosa-linked peripherin-2 mutants,” *Sci. Rep.*, vol. 7, no. 1, pp. 1–13, 2017.
- [114] W. Jiang, A. J. Brueggeman, K. M. Horken, T. M. Plucinak, and D. P. Weeks, “Successful transient expression of Cas9 and single guide RNA genes in *Chlamydomonas reinhardtii*,” *Eukaryot. Cell*, vol. 13, no. 11, pp. 1465–1469, 2014